UC Irvine
Faculty Publications

Title

Seasonal exchange of CO $_2$ and delta ^{18} O-CO $_2$ varies with postfire succession in boreal forest ecosystems

Permalink

Journal

Journal of Geophysical Research, 111(G3)

ISSN

0148-0227

Authors

Welp, L. R
Randerson, J. T
Liu, H. P

Publication Date

2006-09-01

DOI

10.1029/2005JG000126

Supplemental Material

Copyright Information

Peer reviewed

Seasonal exchange of CO_2 and $\delta^{18}O\text{-}CO_2$ varies with postfire succession in boreal forest ecosystems

L. R. Welp,[1] J. T. Randerson,[2] and H. P. Liu[3]

[1] Seasonal cycles of atmospheric CO_2 and $\delta^{18}O\text{-}CO_2$ at high northern latitudes have the potential to serve as indicators of ecological change in response to climate changes. Effective interpretation of these observations requires an understanding of how different species and ecosystems contribute to biosphere-atmosphere exchange. Here we examined the effect of postfire stand age in boreal forest ecosystems on the seasonal distribution of CO_2 and $\delta^{18}O\text{-}CO_2$ fluxes. We measured net CO_2 fluxes in a 3-year burn scar, a 15-year trembling aspen stand, and an 80-year black spruce stand in interior Alaska using eddy covariance. By combining measurements of the oxygen isotopic composition of ecosystem water pools at each stand with measured CO_2 fluxes, we predicted half-hourly $\delta^{18}O\text{-}CO_2$ fluxes and used a one-box atmosphere model to make relative comparisons of the effect of stand age on the shape and amplitude of the seasonal cycle of CO_2 and $\delta^{18}O\text{-}CO_2$. A shorter growing season and higher rates of net ecosystem uptake during midsummer at the 15-year stand resulted in a larger seasonal CO_2 amplitude and a delay in the drawdown of atmospheric CO_2 as compared with the 80-year stand. Reduced levels of gross primary production isoforcing from the 15-year stand during spring and early summer caused atmospheric $\delta^{18}O\text{-}CO_2$ to increase more gradually between April and June as compared with fluxes from the 80-year stand. Our analysis suggests that increased boreal forest disturbance would delay the phase of CO_2 drawdown at high northern latitudes, but would advance the phase of $\delta^{18}O\text{-}CO_2$ drawdown.

Citation: Welp, L. R., J. T. Randerson, and H. P. Liu (2006), Seasonal exchange of CO_2 and $\delta^{18}O\text{-}CO_2$ varies with postfire succession in boreal forest ecosystems, *J. Geophys. Res.*, *111*, G03007, doi:10.1029/2005JG000126.

1. Introduction

[2] Climate change caused by increased greenhouse forcing over the next century is expected to be greatest in arctic and boreal regions, in part from temperature-albedo feedbacks linked with reduced snow and ice cover [*Cess et al.*, 1991; *Arctic Climate Impact Assessment* (*ACIA*), 2004]. Indeed, observed rates of warming in the Arctic over the last few decades have been 50% larger than the global mean [*Intergovernmental Panel on Climate Change* (*IPCC*), 2001], and acceleration of this trend is predicted as greenhouse gas concentrations increase [*ACIA*, 2004]. Evidence that warmer spring temperatures during recent decades have lengthened the terrestrial growing season comes from satellite-derived observations of Normalized Difference Vegetation Index (NDVI) [*Myneni et al.*, 1997; *Tucker et al.*, 2001; *Zhou et al.*, 2001; *Bogaert et al.*, 2002; *Hicke et al.*, 2002; *Nemani et al.*, 2003; *Slayback et al.*, 2003; *Angert et al.*, 2005], passive microwave satellite observations and modeling of soil freeze/thaw transitions [*McDonald et al.*, 2004; *Smith et al.*, 2004], analysis of atmospheric carbon dioxide time series [*Keeling et al.*, 1996; *Randerson et al.*, 1997; *Angert et al.*, 2005], and phenology records [*Walther et al.*, 2002].

[3] The increased growing season length may allow for greater rates of photosynthesis and carbon accumulation during spring and summer [*Frolking et al.*, 1996; *Randerson et al.*, 1999; *Kimball et al.*, 2001; *Myneni et al.*, 2002; *Tanja et al.*, 2003; *White and Nemani*, 2003], whereas warming air and soil temperatures may stimulate higher rates of respiration [*Chapin et al.*, 1996; *Goulden et al.*, 1998]. Warming of northern continental interiors may also increase fire activity [*Stocks et al.*, 1998; *Gillett et al.*, 2004; *Flannigan et al.*, 2005], causing a decrease in the mean age of forests and a shift in species composition. The combined effect of these multiple changes in northern ecosystem processes on biome-level carbon fluxes remains challenging to measure or predict. In this respect, atmospheric trace gas observations have the potential to serve as an important top-down constraint of large-scale ecological change.

[4] The seasonal cycles in concentrations of atmospheric CO_2 and heavy stable isotopologues ($^{13}CO_2$ and $C^{18}OO$) at high northern latitudes integrate carbon fluxes from boreal and arctic biomes across both North America and Eurasia. Thus they record, and have the potential to help diagnose,

---

[1]Environmental Science and Engineering, California Institute of Technology, Pasadena, California, USA.
[2]Earth System Science, University of California, Irvine, California, USA.
[3]Department of Physics, Atmospheric Sciences, and General Science, Jackson State University, Jackson, Mississippi, USA.

terrestrial ecosystem processes and their response to climate change at the biome scale. Here we focus on two of these tracers, CO$_2$ and C^{18}OO, and the sensitivity to species composition of the boreal forests as it varies with postfire stand age. These two tracers are complementary; the seasonal cycle of atmospheric CO$_2$ is sensitive to the net carbon balance of ecosystems, whereas the seasonal cycle of C^{18}OO is sensitive to the magnitude of the gross CO$_2$ fluxes (i.e., photosynthesis and respiration) and the hydrological cycle. Effective use of these tracers as large-scale ecological indicators of climate change [*Menzel and Fabian*, 1999; *Walther et al.*, 2002] requires improved understanding of the processes that control CO$_2$ and C^{18}OO fluxes in northern ecosystems.

[5] Typically, the concentration of CO$_2$ in northern latitudes decreases from May through August, owing to photosynthetic uptake exceeding ecosystem respiration during summer months. Increasing concentrations follow from September through April as a result of slow, continuous ecosystem respiration fluxes to the atmosphere and negligible rates of photosynthesis [*Bolin and Keeling*, 1963]. From the 1960s through the latter part of the 1990s, the seasonal cycle of atmospheric CO$_2$ measured at high northern latitudes increased in amplitude (peak-to-trough) and the phase advanced [*Conway et al.*, 1994; *Keeling et al.*, 1996; *McDonald et al.*, 2004].

[6] Two classes of mechanisms have been proposed to account for the observed changed in the seasonal cycle of CO$_2$. The first involves direct climate controls on the timing and magnitude of northern ecosystem fluxes, including temperature, radiation, the timing of soil thaw, and drought [*Keeling et al.*, 1996; *Randerson et al.*, 1999; *McDonald et al.*, 2004; *Angert et al.*, 2005]. The second involves a change in distribution of plant functional types caused by increases in disturbance [*Zimov et al.*, 1999]. Measurements from Siberian shrub and forest tundra ecosystems show that species assemblages associated with early stages of succession have enhanced rates of photosynthetic uptake during the summer in addition to enhanced respiratory losses during fall, partly from the removal of the less productive and more insulating moss layer. On the basis of these results, *Zimov et al.* [1999] hypothesize that increased disturbance in arctic and boreal biomes has increased the abundance of early successional ecosystems and this, in turn, has contributed to the observed increases in the CO$_2$ seasonal amplitude.

[7] In contrast to the CO$_2$ record, the much shorter C^{18}OO record (measured and reported as δ^{18}O-CO$_2$) shows no unidirectional, fossil fuel–controlled trend (as there is for CO$_2$ and ^{13}CO$_2$) and interannual variability in the annual mean and seasonal amplitude is much larger [*Trolier et al.*, 1996; *Ciais and Meijer*, 1998]. The seasonal cycle and latitudinal gradient of δ^{18}O-CO$_2$ are controlled largely by gross CO$_2$ exchange with the terrestrial biosphere as well as isotopic fractionation of meteoric water and climatic factors such as temperature and humidity [*Francey and Tans*, 1987; *Ciais and Meijer*, 1998; *Peylin et al.*, 1999; *Riley et al.*, 2002; *Cuntz et al.*, 2003a].

[8] When CO$_2$ diffuses into a leaf, it rapidly reaches isotopic equilibrium with the evaporatively enriched leaf water pool because carbonic anhydrase catalyzes CO$_2$ hydration [*Mills and Urey*, 1940; *Farquhar et al.*, 1993;

Yakir and Sternberg, 2000]. Only a portion of the CO$_2$ entering the leaf gets fixed as organic matter before the remainder diffuses back out of the leaf and returns to the atmosphere. This retrodiffusive flux is approximately twice as large as gross primary production and carries the leaf water isotopic signature [*Francey and Tans*, 1987; *Friedli et al.*, 1987; *Farquhar et al.*, 1993]. Similarly, CO$_2$ produced by soil respiration is in contact with soil water for a sufficient time to equilibrate with water in the upper layers of the soil surface before diffusing into the atmosphere [*Hesterberg and Siegenthaler*, 1991; *Tans*, 1998; *Miller et al.*, 1999]. Leaf water is isotopically enriched as compared with soil water because of greater evaporation rates at the leaf surface than the soil surface. As a result, photosynthesis typically enriches atmospheric δ^{18}O-CO$_2$ (more positive) and respiration depletes δ^{18}O-CO$_2$ (more negative) [*Ciais et al.*, 1997]. This large difference between the δ^{18}O of leaf water carried by the photosynthetic CO$_2$ flux and soil water carried by the respiratory CO$_2$ flux, has the potential to be used to partition net CO$_2$ fluxes into one-way gross flux components [*Ogee et al.*, 2004]. Successful partitioning of measured net CO$_2$ fluxes into foliar and soil components using δ^{18}O has been demonstrated at the site level over discrete periods of time during the growing season [*Yakir and Wang*, 1996; *Bowling et al.*, 2003b]. In principle, a similar partitioning at the global scale is possible; however, photosynthetic and respiratory end-members vary widely and are incompletely known.

[9] For both CO$_2$ and δ^{18}O-CO$_2$, the role of different ecosystems and their contribution to biome-level fluxes remain poorly understood. Here we examine the effects of boreal forest postfire stand age on the seasonal cycle of CO$_2$ and δ^{18}O-CO$_2$ using a combination of CO$_2$ flux and oxygen isotope measurements from three stands in a fire chronosequence in interior Alaska. Species composition varies with time since fire and has the potential to influence rates of carbon uptake [*Litvak et al.*, 2003; *Bond-Lamberty et al.*, 2004], respiration rates [*Wang et al.*, 2002; *O'Neill et al.*, 2003], growing season length [*Falge et al.*, 2002], and leaf diffusion properties such as stomatal conductance [*Ewers et al.*, 2005], as well as the use and cycling of meteoric water by the ecosystem [*Flanagan et al.*, 1997]. Each of these differences could lead to changes in the seasonality of CO$_2$ or δ^{18}O-CO$_2$ fluxes. We estimate atmospheric isoforcing for each of our three stands following the approach described by *Flanagan* [2005]. We examine, in detail, differences in biosphere-atmosphere exchange between a deciduous broadleaf forest and an evergreen conifer forest. In a final step, we investigate stand age effects on the seasonal cycles of CO$_2$ and δ^{18}O-CO$_2$ using a one-box atmospheric model. This allowed us to explore the *Zimov et al.* [1999] hypothesis in the context of changes in species composition within boreal forest ecosystems.

2. Site Description

[10] We measured water isotopes and CO$_2$ fluxes at three stands that were part of a fire chronosequence in interior Alaska, near the town of Delta Junction (63°54′N, 145°40′W). This is an area of discontinuous permafrost that experiences seasonal extremes in climate. Temperature measurements at nearby Big Delta (64°00′N, 145°44′W),
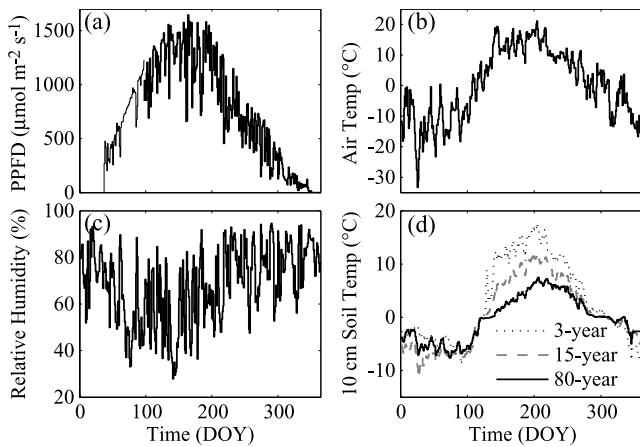
Figure 1. Daily micrometeorological data from Delta Junction during 2002. (a) Daily maximum photosynthetic photon flux density (PPFD), (b) daily mean above canopy air temperature averaged across all stands, (c) daily mean above canopy relative humidity averaged across all stands, and (d) daily mean soil temperature measured 10 cm below the surface at each stand.

from 1937 to 2004 by the Western Regional Climate Center, show the average daily minimum temperature in January was $-24°C$ and the average daily maximum during July was 21°C (Western U.S. climate historical summaries, 2004, Western Regional Climate Center, http://www.wrcc.dri.edu/climsum.html) (hereinafter referred to as WRCC data, 2004). For the 30-year period, from 1971 to 2000, the average annual precipitation in this region was 303 mm and the growing season length (air temperatures above freezing) was approximately 115 days from mid-May to early September (WRCC data, 2004). Our sites were located on relatively well drained silty loam soil [*King et al.*, 2002], and were burned 3 years, 15 years, and approximately 80 years prior to the 2002 growing season. During the summer of 2002, rainfall measured by two tipping bucket rain gauges was 12 mm in May, 66 mm in June, 45 mm in July, 97 mm in August, and 53 mm in September [*Liu et al.*, 2005]. Total precipitation during the 2002 calendar year was approximately 305 mm. Time series of average daily maximum photosynthetic photon flux density (PPFD) above the canopy, relative humidity, and 2 m air temperature are shown in Figure 1, along with soil temperatures at a depth of 10 cm at each stand. Differences in soil temperature between stands were caused partly by differences in canopy structure and leaf area that controlled the amount of shortwave radiation absorbed by the soil/moss surface.

[11] The most recently disturbed stand (the 3-year stand) was burned during the 1999 Donnelly Flats fire (63°54′N, 145°44′W) [*Liu et al.*, 2005]. In 2002, 30% of the ground surface was covered by bunch grasses (*Festuca altaica*) and deciduous shrubs less than 1 m tall. Charred dead spruce boles remained standing and partial moss cover consisted of *Polytrichum* ssp. and *Ceratodon* ssp.

[12] The intermediate aged stand (the 15-year stand) burned during the 1987 Granite Creek fire (63°55′N 145°23′W) and, by 2002, was dominated by an overstory

of deciduous aspen trees (*Populous tremuloides*) with a mean canopy height of 5 m and willow shrubs (*Salix* spp.). The understory vegetation included smaller shrubs (*Ledum palustre*, *Rosa acicularis*, *Vaccinium uliginosum* and *Vaccinium vitisidaea*), grasses (*Festuca* spp. and *Calamagrostis lapponica*) and moss (*Polytrichum* ssp.) [*Liu et al.*, 2005]. The understory also included regrowing black spruce (*Picea mariana*). By 2002, some of the dead spruce boles remained standing, but most had fallen over.

[13] The mature conifer end-member of our study (the 80-year stand) was an approximately 80-year-old stand of black spruce (*Picea mariana*) (63°53′N, 145°44′W), 5 km south of the 3-year stand and less than 20 km southwest of the 15-year stand [*Liu et al.*, 2005]. The mean canopy height was 4 m, and the sparse understory consisted of shrubs (*Ledum palustre*, *Vaccinium uliginosum* and *Vaccinium vitisidaea*). The dominant ground cover was feathermoss (*Pleurozium schreberi* and *Rhytidium rugosum*) and lichen (*Cladonia* spp. and *Stereocaulon* spp.). Moss and fibrous organic layer thickness was approximately 11 cm [*Manies et al.*, 2004].

3. Methods

3.1. Eddy Covariance and Micrometeorological Measurements

[14] Eddy covariance measurements of net ecosystem exchange (NEE) CO$_2$ fluxes were made using an open-path CO$_2$ analyzer (LiCor 7500, LI-COR, Inc., Lincoln, Nebraska) and a 3-D sonic anemometer (CSAT3, Campbell Scientific, Inc., Logan, Utah) at each stand. Vertical and horizontal wind velocity, sonic temperature, and CO$_2$ and water vapor concentrations were recorded at 10 Hz on a Campbell CR5000 data logger. Corrections were made to the CO$_2$ fluxes to account for density effects [*Webb et al.*, 1980] and buoyancy temperature and crosswind effects [*Liu et al.*, 2001]. Energy balance closure during the summer of 2002 (June–August) was 80% at the 3-year stand, 83% at the 15-year stand, and 86% at the 80-year stand [*Liu et al.*, 2005]. Instrument configuration and sampling heights are summarized in Table 1 of *Liu et al.* [2005].

[15] Micrometeorological observations that we used to develop and drive the CO$_2$ flux partitioning and isoflux models included CO$_2$ and latent heat fluxes, wind speed above and inside the canopy, PPFD (LI 190, LI-COR, Inc., Lincoln, Nebraska), precipitation, air temperature and relative humidity above and inside the canopy, and soil temperature at 10 cm depth. Micrometeorological data was 86% complete at the 3-year stand, nearly 100% at the 15-year stand and 95% at the 80-year stand. Air and soil temperature, relative humidity, PPFD, and wind speed data were gap filled using linear interpolation of points surrounding the missing data for short gaps (e.g., less than 3 hours), or using measurements recorded at one of the other nearby tower locations for extended periods of missing data (with the exception of soil temperature which was linearly interpolated for multiday periods of missing data). We filtered NEE measurements for periods of low turbulence using a minimum u^* threshold of 0.2 m s^{-1} [*Goulden et al.*, 1997]. We also excluded periods with rain or dust that potentially interfered with the operation of the infrared gas analyzer. Combined with instrument data gaps, the filtering procedure yielded 30-min NEE measurements for 51% of the growing

season (April–September) at the 3-year stand, 46% at the 15-year stand, and 57% at the 80-year stand.

3.2. Isotopic Measurements

[16] We collected precipitation using rain collectors that consisted of a 7.5-cm-diameter funnel with 20 cm of $^1/_4$ inch ID Tygon tubing feeding into a 500-mL Nalgene bottle. The funnel and bottle were supported inside a PVC pipe. We constructed a vent from 30 cm of $^1/_4$ inch ID Tygon tubing, allowing for rapid filling of the bottle while minimizing fractionation due to evaporation. We emptied the collectors weekly into borosilicate glass vials with screw caps sealed with Parafilm. The vials were stored in a refrigerator until analysis. We collected snow samples from both the top and bottom of the snow pack weekly during winter and stored them in the same way as the summer rain samples. We analyzed precipitation and extracted leaf, stem, and soil water samples for δ^{18}O-H₂O by continuous flow GC-IRMS on a Finnigan MAT Delta S mass spectrometer (Thermo Finnigan, Bremen, Germany) following the method described by *Fessenden et al.* [2002]. We injected 0.5 mL of water by syringe into 7-mL vials flushed with 10% CO₂ in N₂. The vials were capped with Hycar rubber stoppers and allowed to equilibrate by shaking in a 25°C constant temperature water bath for a minimum of 12 hours. We prepared isotopic standards in the same manner as the unknown samples. We used a gas-tight syringe to inject 200–300 μL of headspace into a HP/Agilent Technologies 6890 Series Gas Chromatograph G1530A with a 25-m Poroplot-Q capillary column (0.32 mm diameter). The CO₂ effluent from the GC passed through a Finnigan GC Combustion III and Nafion drying trap before entering the mass spectrometer.

[17] We collected atmospheric water vapor cryogenically by pulling air through a 9-mm OD glass tube cold finger (with an inner 6-mm OD tube) sitting in crushed dry ice. We maintained the flow rate through the cold finger at 0.3 L min^{-1} for approximately 2 hours [*Helliker et al.*, 2002]. Water condensed on the inner portion of the 9-mm tube and the outer portion of the 6-mm tube. Both glass tubes were removed from the dry ice and sampling apparatus and sealed with a rubber stopper/septum and wrapped with Parafilm. Samples were stored in a freezer until analysis. To measure the δ^{18}O of the condensed water vapor, the sample tubes were removed from the freezer and allowed to reach room temperature over a period of 1 to 3 hours. We injected ~1 mL of pure CO₂ through the stopper/septum to bring the internal CO₂ concentration to ~10%. Standards were prepared in 7-mL-headspace vials, as previously described, and both standards and samples were allowed to equilibrate at room temperature for at least 48 hours. We used a gas-tight syringe to inject 80 μL of the headspace from the water vapor tubes into the Delta S GC-IRMS. Sample δ^{18}O-H₂O values were calculated relative to known standards equilibrated at the same time. The reproducibility for this method was ±0.5‰.

[18] We collected bulk soil water samples from soil pits at 2.5, 5, 10, 15, and 30 cm depths, using borosilicate glass vials sealed with Parafilm. We also sampled dominant tree species for stem (xylem) and leaf water isotopic composition. Stems, leaves, and needles collected for isotopic analysis were stored in 25-mL screw-cap borosilicate glass vials and sealed with Parafilm. We collected stem samples from nongreen, woody stems to minimize effects of evaporative enrichment. Stems were cut into 1-cm sections to facilitate water extraction. Petioles were removed from the broadleaf leaves to minimize the effects of non-evaporatively-enriched stem water contributions. Samples were frozen until water was extracted by cryogenic vacuum distillation [*Ehleringer et al.*, 2000].

3.3. Isotopic Modeling of Water Pools

[19] We measured δ^{18}O of atmospheric and ecosystem water pools during two field campaigns in 2002, although to predict the seasonal and annual isoforcing of δ^{18}O-CO₂, we needed continuous estimates of the isotopic composition of the water pools. Therefore it was necessary to model the δ^{18}O of precipitation, water vapor, soil and xylem water, and leaf water at 30-min intervals. We used the measured δ^{18}O of precipitation collected at Delta Junction during 2002 to create a temperature regression based on the mean air temperatures of the week prior to sample collection (because samples were collected weekly) (Figure 2). We compared our isotopic data to four IAEA GNIP stations at Fort Smith (60°02′N, 111°97′W), Mayo (63°37′N, 135°52′W), Whitehorse (60°72′N, 135°52′W), and Yellowknife (62°28′N, 114°27′W), spanning the years 1961–1993 (IAEA/WMO, Global network of isotopes in precipitation, GNIP database, 2004, available at http://isohis.iaea.org). These stations were chosen because they are at similar latitudes as our field sites and also are interior (noncoastal) locations. The regression of weighted monthly δ^{18}O of precipitation on the monthly mean air temperature was nearly identical to that calculated from our own isotopic measurements (Figure 2a). The isotopic temperature dependence from Delta Junction was then applied to the monthly mean air temperature measured at the stands to construct an estimated seasonal cycle of δ^{18}O of meteoric water (Figure 2b). In our model, soil water δ^{18}O was set equal to the δ^{18}O of precipitation. As will be discussed later, this assumption ignores short-term isotopic variations in the top soil layers due to natural variability in precipitation and evaporation between rain events [*Riley et al.*, 2002].

[20] Atmospheric water vapor δ^{18}O was assumed to be depleted relative to modeled precipitation δ^{18}O by −8‰ based on the mean difference between water vapor and precipitation isotopic measurements made during June and August (Figure 3). We also assumed that there was no diurnal cycle in water vapor δ^{18}O on the basis of our measured water vapor δ^{18}O profiles that showed considerable variability, but no clear diurnal trends (data not presented).

[21] Leaf water δ^{18}O becomes enriched during the day owing to evaporative enrichment during transpiration. The level of leaf water enrichment was estimated first using the Craig-Gordon steady state model of isotopic fractionation [*Craig and Gordon*, 1965], expanded to include leaf boundary layer effects [*Flanagan et al.*, 1991]. The steady state ^{18}O/^{16}O ratio of leaf water (H₂^{18}O/H₂^{16}O) at the sites of evaporative enrichment (R_{ss}) is given by

$$R_{ss} = \alpha^* \left[\alpha_k R_{wx} \left(\frac{e_i - e_s}{e_i} \right) + \alpha_{kb} R_{wx} \left(\frac{e_s - e_a}{e_i} \right) + R_a \left(\frac{e_a}{e_i} \right) \right],$$
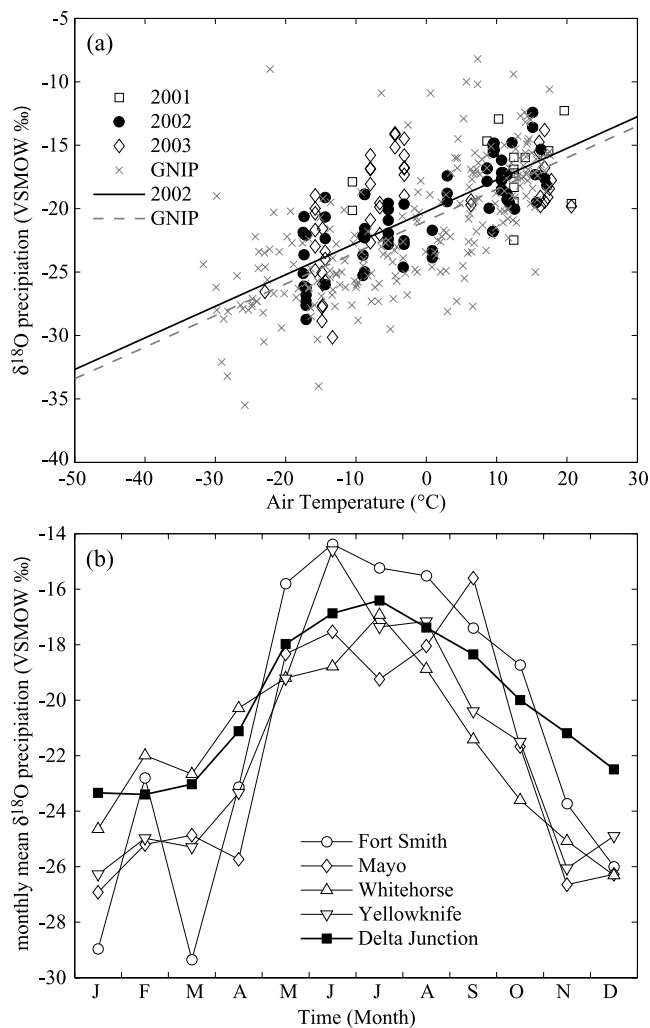
(1)

Figure 2. (a) The $\delta^{18}O$ of precipitation collected at Delta Junction during 2001–2003 as a function of mean air temperature for the week preceding collection. Monthly precipitation data from the GNIP IAEA network stations Fort Smith, Mayo, Whitehorse, and Yellowknife are plotted as a function of monthly mean air temperature. GNIP station time series are intermittent and span from 1961 to 1993. Regressions are shown for 2002 Delta Junction measurements (solid line) and GNIP measurements (dashed line). The temperature regression for 2002 Delta Junction precipitation yielded a slope of 0.25‰/°C and an intercept of −20.22‰, $r^2 = 0.62$, n = 75, p < 0.001. This was similar to the regression for the combined GNIP stations which had a slope of 0.25‰/°C and an intercept of −20.96‰, $r^2 = 0.47$, n = 236, p < 0.001. (b) Monthly mean $\delta^{18}O$ of precipitation for each GNIP station and the estimate for Delta Junction (derived from the temperature regression shown in Figure 2a).

where R_a and R_{wx} are the $^{18}O/^{16}O$ ratios of water vapor in the atmosphere and xylem water respectively and e is the water vapor pressure (subscripts a, s, and i correspond to the free atmosphere, leaf surface and intercellular spaces respectively), α^* is the temperature-dependent equilibrium fractionation factor between liquid water and water vapor, α_k is the kinetic fractionation associated with diffusion of

water vapor in air (1.032) [*Cappa et al.*, 2003] and α_{kb} in the kinetic fractionation associated with diffusion through the boundary layer ($\alpha_{kb} = \alpha_k^{2/3}$). We used the mean 30-min air temperature and relative humidity measured at each stand above the canopy to drive this model of predicted leaf water enrichment.

[22] Measurements of leaf water $\delta^{18}O$ tend to show a lag relative to that calculated with the Craig-Gordon approximation [*Dongmann et al.*, 1974; *Lai et al.*, 2006]. Therefore, we also employed a transitory model where the $\delta^{18}O$ of leaf water is a mixture of the Flanagan modified Craig-Gordon steady state prediction at that time and at the previous time step [*Dongmann et al.*, 1974; *Cuntz et al.*, 2003a; *Lai et al.*, 2006].

$$R_{nss}(t) = R_{ss}(t) - \left[R_{ss}(t) - R_{nss}(t-1)\right] \cdot e^{\left(-\zeta\frac{\Delta t}{\tau}\right)}, \quad (2)$$

where $R_{nss}(t)$ is the non-steady-state prediction of the isotopic ratio of leaf water at time t, $R_{ss}(t)$ is the Craig-Gordon steady state solution at time t, $R_{nss}(t-1)$ is the isotopic ratio of leaf water at time $t-1$, and ζ is represented by the following equation:

$$\zeta = \alpha^*\alpha_{kv}(1-h), \quad (3)$$

where h is the humidity in the canopy air. Here α_{kv} is the effective kinetic fractionation through the stomata and boundary layer ($\alpha_{kv} = 1 - (0.032\ r_s + 0.021\ r_b)/(r_s + r_b)$ where r_s and r_b are the stomatal and boundary layer resistances to water vapor diffusion, and 0.032 and 0.021 are scalars corresponding to the respective isotopic fractionation factors) [*Cappa et al.*, 2003].

[23] The turnover time of leaf water (τ in equation (2)) is proportional to the volume of leaf water divided by the transpiration rate and Δt is the 30-min time step of the model. We used a τ of 2 hours based on reducing residuals between measured and modeled leaf water values. Leaf water turnover time probably varies with species and should vary diurnally
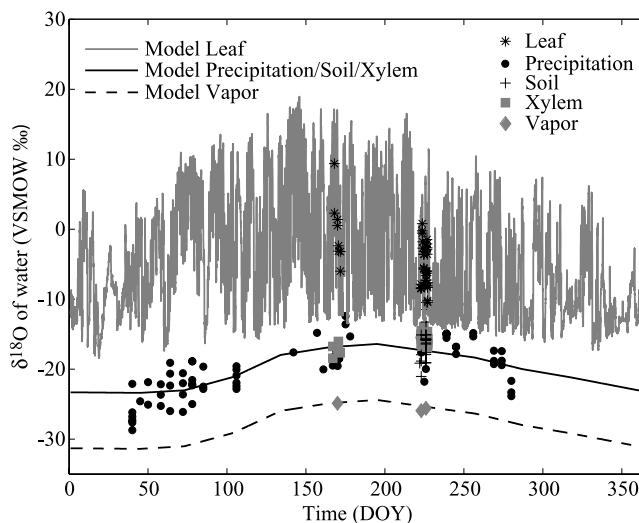

Figure 3. Measured (symbols) and modeled (lines) $\delta^{18}O$ of leaf water, precipitation, soil, and xylem water, and water vapor for the year 2002.

Table 1. Model Parameters Used to Partition NEE Into GPP and R_e Components

Stand	Q_{10},[a] Unitless	R_o,[a,b] μmol CO_2 m^{-2} s^{-1}	$AMAX$,[c] μmol CO_2 m^{-2} s^{-1}	α[c,d] mol CO_2/mol photons	$FPAR$,[c] %
3-year	2.1	1.0	−3.6	−0.04	60
15-year	3.9	2.3	−11.2	−0.08	84
80-year	4.7	5.0	−9.6	−0.09	84

[a]Q_{10} and R_o are solved using 10-cm soil temperatures.
[b]R_o was separately estimated for 5-day intervals during the growing season; here we report the mean over the growing season.
[c]$AMAX$, α and $FPAR$ are June–August means.
[d]The units are per mol of absorbed photons (incident $PPFD \times FPAR$).

with transpiration rate; however, we had limited data to make this evaluation and therefore decided to use a constant τ for all stands. For comparison, *Cuntz et al.* [2003a] used a τ of ∼3 hours globally, and *Lai et al.* [2006] solved for a τ of 11 hours for conifers in the Pacific Northwest.

3.4. Partitioning CO_2 Fluxes

[24] NEE measurements at each stand were partitioned into ecosystem respiration (R_e) and gross primary productivity (GPP) components using Q_{10} and Michaelis-Menten models, respectively. We used a temperature dependent Q_{10} respiration model that was mathematically equivalent to a Van't Hoff exponential model [*Lloyd and Taylor*, 1994].

$$R_e = R_o Q_{10}^{\left(\frac{T-T_o}{10}\right)}, \qquad (4)$$

where T is the 10-cm soil temperature, $T_o = 10°C$, R_o is the base respiration rate and Q_{10} is a temperature sensitivity parameter. Nighttime growing season (April–September) NEE measurements and 10-cm soil temperatures from 3 years of combined measurements (2002–2004) were used to solve for stand-specific Q_{10} values. Using these Q_{10} values and nighttime NEE measurements, we then solved for R_o values during 15-day windows moving by 5-day increments during the growing season (April–September). Winter R_e was predicted by using the growing season Q_{10} and half the mean growing season R_o. For each stand, these R_o and Q_{10} values were used with 10-cm soil temperature to estimate R_e at the half-hourly time step of our model.

[25] Gross primary production (GPP) was modeled after *Zha et al.* [2004],

$$GPP = \left(\frac{A_{max} \cdot \alpha \cdot APAR}{A_{max} + \alpha \cdot APAR}\right) \cdot VPD_{scalar}, \qquad (5)$$

where $APAR$ (μmol photons m^{-2} s^{-1}) is absorbed photosynthetically active radiation ($APAR = PPFD \times FPAR$, where $FPAR$ is the fraction of PAR absorbed by the vegetation), GPP and A_{max} (maximum photosynthetic capacity) are both in μmol CO_2 m^{-2} s^{-1} and α is a quantum efficiency (mol CO_2/mol photons). Many studies have explored the effect of vapor pressure deficit (VPD) and humidity levels on leaf-level gas exchange [*Jarvis and McNaughton*, 1986]; therefore we included a dependence on VPD in the assimilation model to better represent diurnal variations in water stress. (This VPD_{scalar} was not included by *Zha et al.* [2004].)

$$VPD_{scalar} = 1 - 0.5\left(\frac{VPD}{VPD_{max}}\right). \qquad (6)$$

The value of VPD_{scalar} (unitless) decreased linearly with increasing VPD until reaching VPD_{max}, above which it remained constant at 0.5. For each stand, we fixed VPD_{max} at 3 kPa. This resulted in a very conservative reduction of GPP during afternoon periods of high VPD. The GPP model behaves linearly when $\alpha \times APAR$ is much smaller than A_{max} and saturates when $\alpha \times APAR$ approaches A_{max}. A_{max} and α were solved for every week during the growing season using $PPFD$ data recorded by the micrometeorological towers and $FPAR$ derived from MODerate Resolution Imaging Spectroradiometer (MODIS) observations [*Myneni et al.*, 2002]. Table 1 lists values of the model parameters for each stand used to calculate GPP and R_e fluxes for 2002.

3.5. Atmospheric Modeling

[26] We used a simple one-box atmosphere model to isolate the relative effect ecosystem exchange from each forest type has on the seasonal cycle of CO_2 and $\delta^{18}O$-CO_2 of the atmosphere. The atmospheric box represents the high northern latitude atmosphere in which one age class of forest (e.g., the 3-year stand, the 15-year stand, or the 80-year stand) interacts with the atmosphere in each model run. The mass of air in the atmospheric box (M_a in equations (7) and (8)) was defined so that the amplitude of the seasonal cycle of CO_2, when forced with the fluxes from the 80-year stand, matched the amplitude at the Point Barrow station of the NOAA CMDL network [*Conway et al.*, 1994]. M_a was the same for each stand and model simulation. The conceptual experiment presented here is roughly equivalent to covering the entire boreal forest land area with a single age class of forest, and mixing the resulting biospheric fluxes into the entire atmosphere contained between 59°N and 70°N. Observations at the Point Barrow station represent well-mixed background values of CO_2 and $\delta^{18}O$-CO_2 at high northern latitudes (because gases are sampled from ocean wind sectors under well-mixed conditions) and will be used later to give a reference framework for our results. No atmospheric boundary conditions were imposed (i.e., there was no mixing from other latitudes). The change in atmospheric CO_2 is predicted from modeled R_e and GPP fluxes (mol m^{-2} 30 min^{-1}) starting with an atmospheric CO_2 concentration at 370 ppm.

$$\frac{d(C_a M_a)}{dt} = GPP + R_e, \qquad (7)$$

where C_a is the molar ratio of CO_2 in the one-box model, and M_a is the mass of air in the atmospheric box (equivalent to 5.4×10^5 mol air m^{-2}).

[27] To determine the total isotopic effect of biospheric CO_2 fluxes on the atmosphere, net isofluxes (in units of moles C ‰) were calculated at half-hour time steps as

$$\frac{d\left(C_a M_a \delta_a^{CO_2}\right)}{dt} = GPP\left(\delta_{a,i}^{CO_2} - \Delta_A\right) + R_e\left(\delta_{soil}^{CO_2} - \varepsilon_{diff}\right), \quad (8)$$

where $\delta_a^{CO_2}$ is the $\delta^{18}O$ of CO_2 in the one-box model (initialized at -1.4‰ VPDB-CO_2), $\delta_{a,i}^{CO_2}$ is the $\delta^{18}O$ of atmospheric CO_2 used in calculating the isofluxes and equivalent to the mean seasonal cycle of observations from the Point Barrow NOAA CMDL station, Δ_A is the discrimination against $C^{18}OO$ during photosynthesis (defined later in equation (9)), $\delta_{soil}^{CO_2}$ is the $\delta^{18}O$ of CO_2 in equilibrium with soil water (‰ VPDB-CO_2), and ε_{diff} is the fractionation associated with diffusion of CO_2 out of the soil (‰).

[28] The seasonal cycle of $\delta_a^{CO_2}$ was determined by dividing equation (8) by equation (7). For this modeling study, ε_{diff} was assumed to be -7.2‰ [*Miller et al.*, 1999]. We assumed that the abiotic retrodiffusion isoflux [*Stern et al.*, 2001] did not contribute to the seasonality in $\delta^{18}O$-CO_2. The discrimination associated with GPP, Δ_A, was first presented by *Farquhar et al.* [1993] and has been modified by *Gillon and Yakir* [2001] to include the effect of incomplete isotopic equilibration of CO_2 with H_2O by carbonic anhydrase. *Gillon and Yakir* [2001] showed that in most cases, hydration of CO_2 by carbon anhydrase is not 100% efficient, and some of the CO_2 that diffuses into the leaf returns to the atmosphere without isotopically equilibrating with leaf water. Although this effect is more pronounced in C_4 grasses, where carbonic anhydrase is only about 40% efficient, it is estimated to be approximately 88–99% for broadleaf and conifer C_3 trees.

$$\Delta_A = \bar{a} + \varepsilon\left[\theta_{eq}\left(\delta_c^{CO_2} - \delta_{a,i}^{CO_2}\right) - \bar{a}\frac{(1-\theta_{eq})}{(\varepsilon+1)}\right] \quad (9)$$

$$\varepsilon = \frac{C_c}{(C_a - C_c)}. \quad (10)$$

Here $\bar{a}$ is the weighted mean of discrimination occurring during diffusion from ambient air to the sites of carboxylation in the chloroplast (estimated to be 7.4‰) and $\delta_c^{CO_2}$ is the oxygen isotopic composition of CO_2 (‰ VPDB-CO_2) in the chloroplast. The $\delta_c^{CO_2}$ is assumed to be in isotopic equilibrium with enriched leaf water at the ambient air temperature (close to leaf temperature). The fraction of CO_2 entering the leaf that fully equilibrates with the leaf water pool before exiting is denoted as θ_{eq} For the 3-year and 15-year stands, we used the mean of the ranges of values given for trees/shrubs by *Gillon and Yakir* [2001], $\theta_{eq} = 0.96$. Likewise, for the 80-year stand, the mean for conifers was $\theta_{eq} = 0.93$. C is the partial pressure of CO_2 and the subscripts a and c correspond to the CO_2 in ambient air and inside the choloroplast. We used the internal stomatal CO_2 ratio with the ambient CO_2 mixing ratio (C_i/C_a) as an estimate of C_c/C_a used to calculate ε (equation (10)). We recognize that this is a simplification given that there is evidence that C_i and C_c can differ by $0.1 \times C_a$ to $0.2 \times C_a$ [*Lloyd and Farquhar*, 1994; *Yakir and Sternberg*, 2000;

Cuntz et al., 2003a]. To address this, we conducted a sensitivity analysis in which we varied C_i and examined the impacts on $\delta^{18}O$-CO_2 isofluxes. C_i/C_a ratios were estimated from $\delta^{13}C$ of plant tissue collected in the summer of 2002 using the relationship for C_3 plants derived by *Farquhar et al.* [1989]. The $\Delta^{13}C$ discrimination was estimated at 20.9‰ for dominant grasses at the 3-year stand, 22.0‰ for aspen at the 15-year stand, and 21.2‰ for black spruce at the 80-year stand. This translates to C_i/C_a ratios (or C_c/C_a estimates) of 0.71, 0.76 and 0.73, respectively. These estimates are broadly consistent with *Dang et al.* [1997] measurements of 0.81 for aspen and 0.71 for black spruce. Because the value of C_c/C_a sets the magnitude of the retrodiffusive flux of CO_2 out of the leaf and to the atmosphere, we wanted to include the effects of the diurnal cycle of C_c/C_a in our isoforcing calculations. We introduced a diurnal cycle in C_i/C_a (used to estimate C_c/C_a) using the Ball-Berry equation [*Ball*, 1988].

$$\frac{1}{r_s} = \frac{m \cdot GPP \cdot h_s \cdot P}{C_s} + b, \quad (11)$$

and a rearrangement of the diffusion representation of photosynthesis.

$$\frac{C_i}{C_a} = 1 + \frac{GPP \cdot P \cdot (1.65 r_s + 1.37 r_b)}{LAI \cdot C_a}. \quad (12)$$

In the preceding two equations, r_s is the resistance of water through the stomata (m^2 s μmol⁻¹ H_2O), and r_b is resistance through the laminar leaf boundary layer (m^2 s μmol⁻¹ H_2O). C_s and C_a are the partial pressures of CO_2 at the leaf surface (including the effect of r_b) and in the atmosphere, h_s is relative humidity at the leaf surface, b is the residual conductance when GPP is zero, P is the atmospheric pressure and LAI is the unitless leaf area index which varies seasonally (from MODIS observations) and m is a constant. We solved for parameters m and b in equation (11) such that when entered into equation (12), the GPP-weighted annual mean C_i/C_a for each stand matched our estimates from the $\Delta^{13}C$ measurements. The sensitivity of the seasonal cycle of $\delta^{18}O$-CO_2 to the diurnal cycle of C_i/C_a will be explored further in this paper.

[29] In previous modeling studies, $\delta_a^{CO_2}$ and $\delta_{a,i}^{CO_2}$ have been "coupled" so that the model-predicted $\delta^{18}O$-CO_2 from the previous time step was used to calculate the discrimination in the next time step. We found it necessary to fix $\delta_{a,i}^{CO_2}$ in equations (8) and (9) with observations from Point Barrow (rather than allowing it to change in response to the stand model isoforcing). This was necessary because atmospheric CO_2 is not in isotopic equilibrium with the extremely negative $\delta^{18}O$ of water pools at high northern latitudes. In the coupled simulations that we first attempted, $\delta_{a,i}^{CO_2}$ would reach values as negative as -4 to -5‰ (VPDB-CO_2) by the end of 1 year because our model did not include mixing with air enriched in $\delta^{18}O$-CO_2 from the tropics. Because the calculated isofluxes were dependent on $\delta_{a,i}^{CO_2}$, (through Δ_A in equation (9)) it was necessary to keep $\delta_{a,i}^{CO_2}$ consistent with current high-latitude observations to produce realistic fluxes. The discussions of our model results will be based on the resulting model-predicted $\delta_a^{CO_2}$. Note that removing the seasonal cycle and using a constant value for $\delta_{a,i}^{CO_2}$ for

the entire year (Point Barrow annual mean of $-1.4‰$) yielded nearly identical results and did not change any of the conclusions of this study.

[30] The purpose of the simple atmospheric model was to examine in isolation how biosphere-atmosphere fluxes that vary with stand age influence the atmospheric record. This approach provides insight about the role of species composition within boreal forests, and is not meant to replace a more realistic coupled biosphere-atmosphere model that includes atmospheric transport and fluxes from the ocean, stratosphere, fossil fuels, and other terrestrial ecosystems.

[31] We linearly detrended our model results of seasonal cycles of CO_2 and $\delta_a^{CO_2}$ (referred to as modeled $\delta^{18}O$-CO_2) to allow us to compare seasonal phasing across stands and with atmospheric observations. This is a common first step in the analysis of the seasonal cycle for atmospheric trace gases that also have a secular trend; it was required here because our local ecosystem fluxes were not in steady state with the atmosphere.

4. Results

4.1. CO_2 Fluxes

[32] Measurements of NEE from the three stands are shown in Figure 4. In the spring, the onset of photosynthesis and net CO_2 uptake was delayed by approximately 3 weeks at the 15-year stand as compared with the 80-year stand. Leaf emergence of aspen at the 15-year stand occurred between 18 and 24 May 2002, day of year (DOY) 138–144. By DOY 146, the daily net CO_2 flux was negative. The carbon uptake period, as defined by negative daily net CO_2 fluxes, was significantly shorter at the younger stands; the 3-year stand was reduced by 9 weeks as compared to the 80-year stand and the 15-year stand was reduced by 7 weeks.

[33] In midsummer from 18 June to 15 July 2002 (DOY 169–196), mean midday NEE (1000–1400 local solar time) was -1.2 μmol m^{-2} s^{-1} at the 3-year stand, -5.7 μmol m^{-2} s^{-1} at the 15-year stand, and -4.2 μmol m^{-2} s^{-1} at the 80-year stand. For this same period, integrated daily NEE was -0.3 g C m^{-2} d^{-1} at the 3-year stand, -2.4 g C m^{-2} d^{-1} at the 15-year stand, and -1.3 g C m^{-2} d^{-1} at the 80-year stand. Both the midday minima and daily NEE were reduced at the 3-year stand because of low leaf area. Midday NEE (1000–1400 local solar time) was 36% more negative at the 15-year stand than at the 80-year stand. Integrated over 24 hours, the difference was even larger. The daily NEE for the 15-year stand was 85% more negative because during the night, NEE fluxes from the two stands were similar in magnitude and offset the differences measured during midday.

[34] The R_e and GPP models described in the methods section were combined to form modeled half-hour NEE flux estimates. Weekly composite averages of the modeled fluxes are plotted with tower NEE diurnal averages in Figure 4. The model slightly underpredicted the nighttime NEE maxima and the daytime NEE minima (Figure 4). Our calculated Q_{10} values (Table 1) were between 2.1 to 4.7, and are within the range of Q_{10} values reported for other boreal forest ecosystems [*Wang et al.*, 2002].

[35] The magnitude of the potential bias between the modeled and measured NEE during the growing season was examined by comparing differences in the cumulative
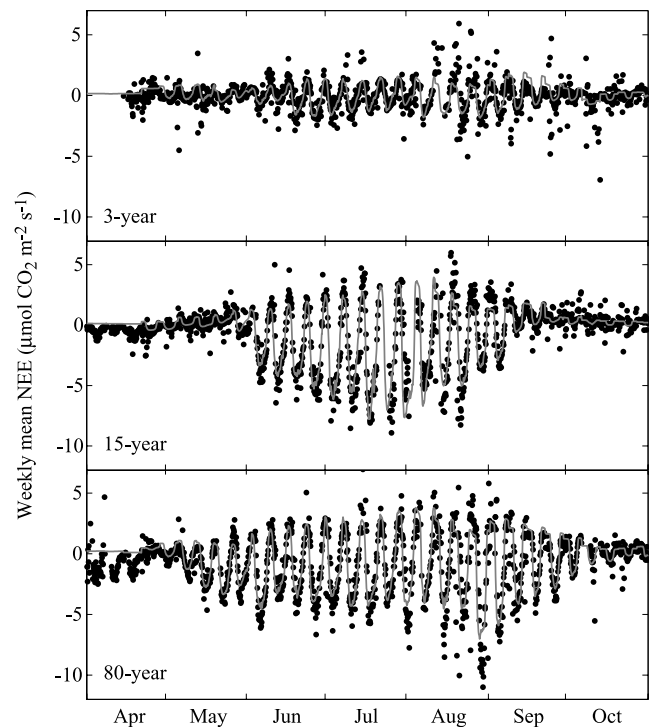

Figure 4. Measured (black solid circles) and modeled (solid grey line) weekly mean NEE for the three stands in 2002. This plot shows mean diurnal cycles constructed from 7-day intervals of 30-min NEE data. The mean diurnal cycles are plotted sequentially to allow examination of the seasonality in GPP (indicated partly by the daytime minima) and R_e (indicated partly by the nighttime maxima). The growing season at the 15-year stand is shorter and more intense (with a larger diurnal cycle in midsummer). Linear regression slopes between modeled and measured (weekly mean) NEE are 0.18 at the 3-year stand ($r^2 = 0.35$), 0.75 at the 15-year stand ($r^2 = 0.76$) and 0.59 at the 80-year stand ($r^2 = 0.72$). CO_2 fluxes at the 3-year stand are small, making them difficult to measure and model and resulting in poor correlation statistics.

NEE (DOY 100–300) of the model fluxes with tower-measured NEE (Figure 5a). These results showed that the modeled NEE fluxes underpredicted the carbon uptake at each stand; however, without adding more complexity to our partitioning model, we considered this a reasonable fit to observations because it captured most of the seasonal change in net CO_2 fluxes (shape of the curves in Figure 5a) as well as variations in the diurnal cycle (Figure 4). Although the modeled NEE fluxes should be used cautiously, especially in the winter, the integrated annual sums provided an estimate of the magnitude of the source or sink of CO_2 at each stand for the entire year (Figure 5b). Annual integrated sums of GPP and R_e, in addition to NEE, are summarized in Table 2.

4.2. Observations and Modeling of the $\delta^{18}O$ of Water Pools

[36] Figure 3 shows the range of precipitation, soil, xylem, leaf and water vapor isotope measurements from field campaigns during 2002, along with model estimates.
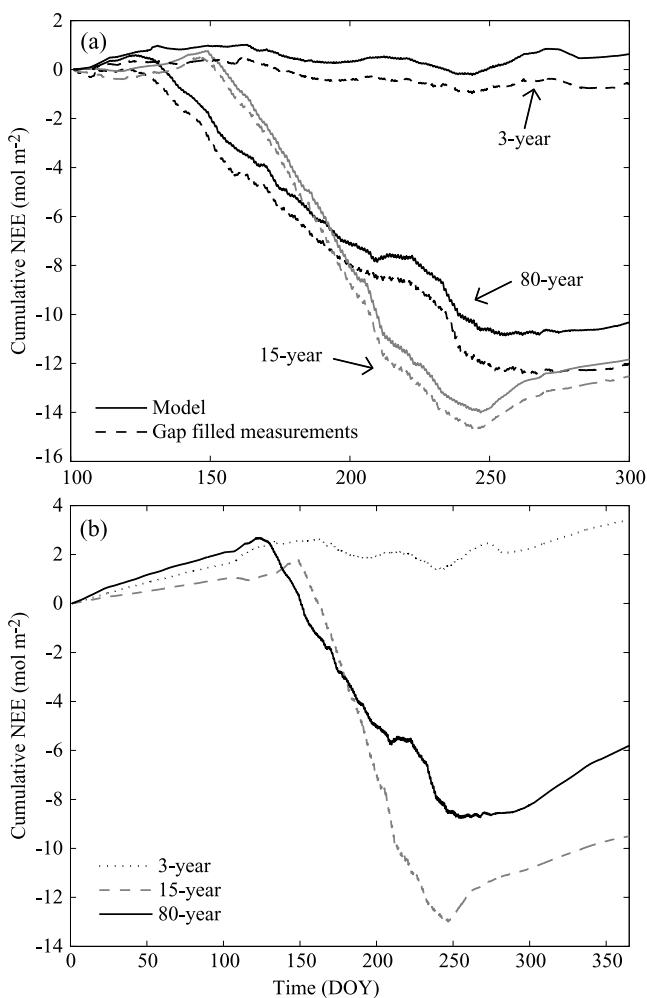
Figure 5. (a) A comparison between modeled NEE and measured NEE during the growing season, DOY 100−300. The solid lines are cumulative modeled NEE estimates, and the dotted lines are measured NEE values that were gap-filled with modeled estimates during periods of missing data. Modeled NEE has a bias toward decreased net carbon uptake at each stand. (b) Cumulative modeled NEE (starting at DOY 1) for the 3-year stand, 15-year stand, and 80-year stand. The sign convention is such that positive values are fluxes to the atmosphere and negative values are uptake by the ecosystem. The 3-year stand was a source with a flux of approximately 3.4 mol CO$_2$ m^{-2} yr^{-1} (40.8 g C m^{-2} yr^{-1}) while the 15-year stand was a sink with a flux of approximately −9.5 mol CO$_2$ m^{-2} yr^{-1} (−114 g C m^{-2} yr^{-1}). The mature 80-year stand was closer to steady state, but was still a sink of CO$_2$ with a flux of approximately −5.8 mol CO$_2$ m^{-2} yr^{-1} (−69.6 g C m^{-2} yr^{-1}).

During the day, bulk leaf water δ^{18}O was substantially enriched as compared to δ^{18}O of precipitation. At night, non-steady-state estimates of leaf water δ^{18}O decreased but did not fully return to xylem water values. Field measurements of δ^{18}O of water vapor during midsummer ranged between −18‰ to −29‰ and the daily averages were approximately 6−9‰ less than the model predicted δ^{18}O of precipitation (Figure 3). Each vapor δ^{18}O value plotted is an average of vertical canopy profiles measured four times

Table 2. Annual Ecosystem Fluxes, Isofluxes, and Other Model Parameters

Annual Value, Flux-Weighted[a]	3-Year	15-Year	80-Year	Units
GPP	−16.1	−36.3	−41.2	mol m^{-2} yr^{-1}
R$_e$	19.5	26.8	35.5	mol m^{-2} yr^{-1}
NEE	3.4	−9.5	−5.8	mol m^{-2} yr^{-1}
δ^{18}O leaf water (GPP)	−0.6	−1.4	−0.5	‰ (VSMOW)
δ^{18}O soil water (R$_e$)	−18.3	−17.8	−18.1	‰ (VSMOW)
δ^{18}O leaf CO$_2$ (GPP)	1.6	0.3	1.6	‰ (VPDB-CO$_2$)
δ^{18}O soil CO$_2$ (R$_e$)	−15.4	−14.5	−14.1	‰ (VPDB-CO$_2$)
C$_c$/C$_a$ (GPP)	0.71	0.76	0.73	unitless
Δ$_A$ (GPP)	9.3	5.1	7.5	‰
GPP·(δ$_{a,i}^{CO_2}$ − Δ$_A$)	170	227	360	mol m^{-2} yr^{-1} ‰
R$_e$·(δ$_{soil}^{CO_2}$ − ε$_{soil}$)	−441	−581	−753	mol m^{-2} yr^{-1} ‰
Net Isoflux	−271	−354	−393	mol m^{-2} yr^{-1} ‰

[a]Gross fluxes used for parameter flux weighting are in parentheses.

over the course of 1 day. To examine the model performance, measurements of leaf and xylem water from field campaigns in June and August are expanded along with model predictions in Figure 6. The different stand ages
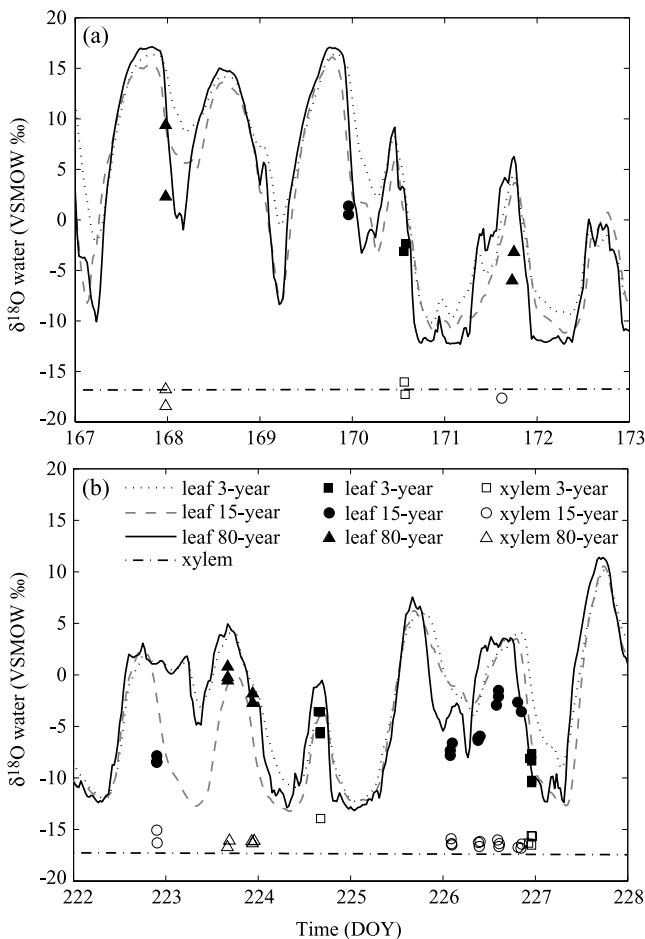

Figure 6. Measured δ^{18}O of leaf water and xylem water (symbols) are shown with model predictions (lines) during intensive field campaigns during (a) 16−22 June 2002 and (b) 10−16 August 2002. The leaf water model used in this study was a non-steady-state model with a leaf water turnover time of 2 hours. Modeled xylem water was set equal to the δ^{18}O of precipitation.

show similar modeled leaf water $\delta^{18}O$ because of similarities in climate driver datasets (i.e., air temperatures, wind speeds, and relative humidity levels were similar at all three stands). The model did reasonably well at capturing the magnitude and diurnal variability of leaf water $\delta^{18}O$, but overestimated enrichment levels on several days. Relative humidity contributed the most to variability in the leaf water $\delta^{18}O$ model predictions over weekly to monthly timescales. The seasonal maximum in leaf water isotopic enrichment (DOY $\sim$150 in Figure 3) was linked to the seasonal minimum in relative humidity (DOY $\sim$150 in Figure 1) and not to the seasonal maximum in $\delta^{18}O$ of modeled plant source water (precipitation) which occurred near DOY 200 in Figure 3.

4.3. Atmospheric Modeling

[37] The shorter and more intense growing season at the 15-year deciduous aspen stand caused a 30% increase in the peak-to-trough CO_2 seasonal amplitude, a delay in maximum CO_2 concentration, and an advance in minimum CO_2 concentration compared to the 80-year stand (Figure 7a). The "downward zero crossing time" of the phase (the day which the CO_2 concentration crosses the mean value of the seasonal cycle in its descending phase) was delayed by 13 days at the 15-year stand as compared with the 80-year stand. The amplitude of the seasonal cycle at the 3-year stand was small and was difficult to separate from the secular trend. The downward zero crossing time analysis for the 3-year stand yielded a delay of 9 days compared to the 80-year stand, however, small NEE fluxes at the 3-year stand substantially increased the error of the model prediction.

[38] Although we did not necessarily expect the one-box model results to match atmospheric observations because of the lack of transport in the model, we compared the box model results of CO_2 (and later $\delta^{18}O$-CO_2) with the mean seasonal cycle of flask measurements from Point Barrow, Alaska, in Figure 7a. The 80-year stand exhibited a maximum in CO_2 in April close to the atmospheric observations, but the predicted minimum in September was delayed from observations by 1 month. The 15-year stand most closely matched the atmospheric observations with an identical spring maximum in May and minimum in August. The seasonal amplitude in CO_2 agreed well with observations because the mass of air in the one-box model was chosen so that the 80-year stand fluxes matched this feature of the atmospheric record. We used the same mass for the other two model simulations.

[39] To understand effects of photosynthesis and respiration on atmospheric $\delta^{18}O$-CO_2, we considered the isotopic flux (or isoforcing) of each component separately (Figure 8). As described previously, photosynthesis normally enriches the atmosphere in $\delta^{18}O$-CO_2, and respiration depletes the atmosphere. The large changes in isoforcing were constrained to periods of the year where there were large CO_2 fluxes, as the isoflux is the product of the one-way CO_2 flux and the isotopic composition of this flux. The combined net isoforcing on the atmosphere is shown in Figure 9. In terms of total net isoforcing, the 3-year stand had the effect of relative enrichment compared to the mature 80-year stand (also see Table 2). Although the recent fire disturbance at the 3-year stand decreased the atmospheric enrichment due to reduced assimilation, it diminished the
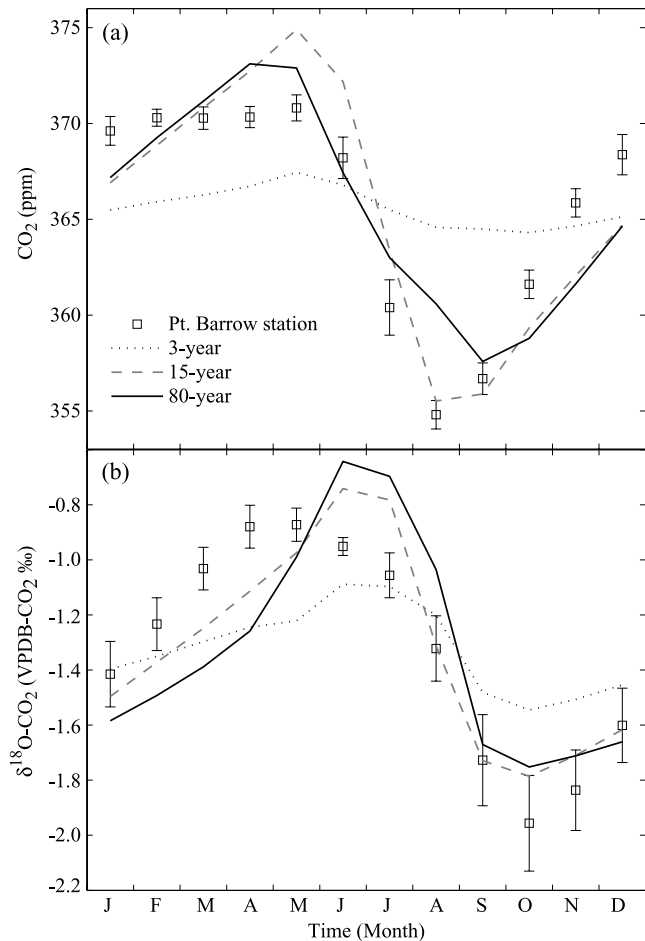

Figure 7. Predicted seasonal cycles of (a) CO_2 and (b) $\delta^{18}O$-CO_2 for fluxes from each stand compared to the mean seasonal cycle of the NOAA CMDL flask network observations at Point Barrow (1990–1997). Error bars on the Point Barrow observations represent the standard deviation of each mean monthly value for the entire data record. The phase of the 15-year CO_2 seasonal cycle is delayed relative to that at the 80-year stand and the amplitude is increased. In contrast, the phase of 15-year $\delta^{18}O$-CO_2 seasonal cycle is advanced relative to that predicted for the 80-year stand.

depletion by reducing respiration even more. The overall effect was to enrich the atmosphere in $\delta^{18}O$-CO_2 relative to the 80-year stand. The intermediate 15-year stand had a net isoforcing that was not substantially different from the 80-year stand.

[40] Using the modeled isofluxes for each forest, a seasonal cycle of $\delta^{18}O$-CO_2 was predicted using the simple one-box model ($\delta_a^{CO_2}$) (Figure 7b). Since this is not a fully coupled model, the model results of $\delta^{18}O$-CO_2 reflect isoforcing by each forest age stand prior to feedbacks with the atmosphere. All three stands exhibited maximum $\delta^{18}O$-CO_2 in June and minimum in October. The zero crossing point of the seasonal cycle of the younger stands was advanced by 12 days relative to the 80-year stand (Figure 7b). The shape of the $\delta^{18}O$-CO_2 seasonal cycle during spring and early summer is also noticeably different between the 15-year and 80-year stands. In part because of

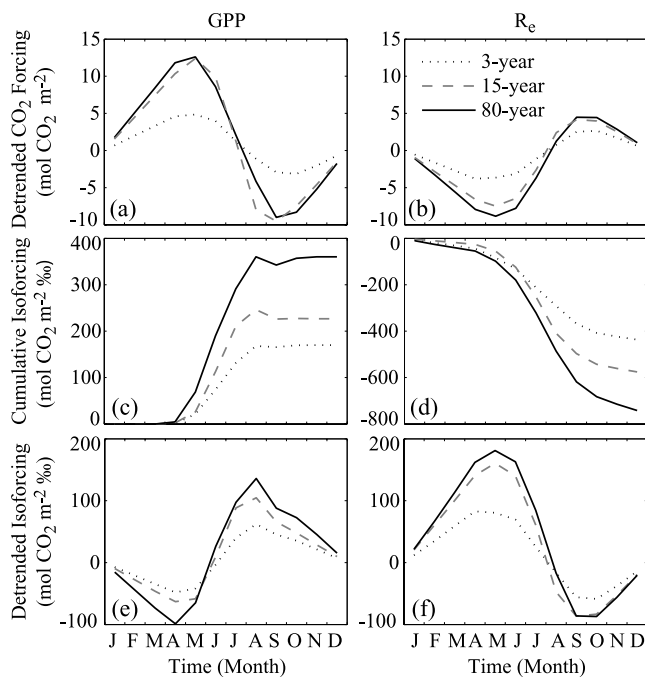**Figure 8.** Cumulative (a) GPP and (b) R_e components of CO_2 forcing with the annual trend removed, (c) GPP and (d) R_e cumulative isoforcing, and (e) GPP and (f) R_e cumulative isoforcing with the annual trend removed. Note that the y-axis units in Figures 7a, 7b, 7e, and 7f are relative units; they are not absolute values. At no time during the year is the cumulative GPP isoforcing negative (Figure 7c) nor is the cumulative R_e isoforcing positive (Figure 7d).

the earlier onset of photosynthesis at the 80-year stand (Figure 4) that coincided with relatively low levels of humidity (Figure 1), this stand had substantially greater GPP isoforcing during May and June (Figure 8). As a consequence, $\delta^{18}O$-CO_2 increased more rapidly from April to June for the 80-year stand than for the 15-year stand. Figure 7b also compares model predictions to atmospheric observations at Point Barrow, Alaska, the same values ($\delta_{a,i}^{CO_2}$) used to calculate the photosynthetic discrimination in equations (8) and (9). By comparing the detrended seasonal cycles of GPP and R_e components of the net isoforcing (Figures 8e and 8f), it is clear that isotopic exchange associated with R_e has a larger effect on the seasonal cycle than isotopic exchange associated with GPP.

4.4. Sensitivity of the $\delta^{18}O$-CO_2 Seasonal Cycle to C_c/C_a

[41] We examined the sensitivity of the predicted seasonal cycle of $\delta^{18}O$-CO_2 amplitude and phase to the C_c/C_a ratio used in our model. For clarity, we present results for the 15-year stand only; however, similar results were obtained for the other stands. First, we tested the importance of the diurnal cycle in C_c/C_a by comparing model results from our standard approach (that included a diurnally variable C_c/C_a predicted using the Ball-Berry equation) with a model run that had a time-invariant C_c/C_a value set at the GPP-weighted annual average of the variable case (i.e., GPP weighted C_c/C_a was the same in both runs). The constant C_c/C_a case enriched the atmosphere $\delta^{18}O$-CO_2 compared to

the variable C_c/C_a case by doubling the GPP isoforcing and decreased the amplitude by 33% (Table 3). The increased GPP isoforcing component also delayed the zero point crossing by 17 days.

[42] This sensitivity was a result of the covariance of leaf water $\delta^{18}O$ enrichment and C_c/C_a over a diurnal cycle. During midday when leaf water was most enriched, there were two negative feedbacks that limited GPP isoforcing. First, if there was no change in stomatal conductance, as GPP rates increased, C_c/C_a decreased, reducing the magnitude of the retrodiffusive flux. Second, stomatal conductance often decreased during midday in response to low levels of atmospheric humidity, and this also reduced C_c/C_a. Diurnal covariance between afternoon leaf water enrichment and decreased C_c/C_a was critical for predicting the GPP isoforcing component (equations (9) and (10)), and hence the seasonal cycle of $\delta^{18}O$-CO_2. *Cuntz et al.* [2003a] also recognized the importance of C_c/C_a (or similarly, C_i/C_a) and noted that reasonable values of C_c/C_a could easily adjust the magnitude of the GPP isoforcing (through ε in equation (10)) by a factor of 2 ($C_c/C_a = 0.67$) or 3 ($C_c/C_a = 0.75$). We show here that it is possible to increase the GPP isoforcing by a factor of 2 without changing the GPP weighted C_c/C_a annual mean, but by simply removing the diurnal cycle in C_c/C_a.

[43] The results from the sensitivity tests where we adjusted the C_c/C_a weighted mean value by ±0.1 were unexpected. Instead of increased C_c/C_a leading to an increase in the GPP isoforcing through the ε factor included in Δ_A, it led to a small decrease. This was because for part of the year, $\delta^{18}O$ of leaf CO_2 was greater than the $\delta^{18}O$ of the atmosphere (positive GPP isoforcing) and for part of the year $\delta^{18}O$ of leaf CO_2 was less than $\delta^{18}O$ of the atmosphere (negative GPP isoforcing) (Figure 10). In effect, the C_c/C_a
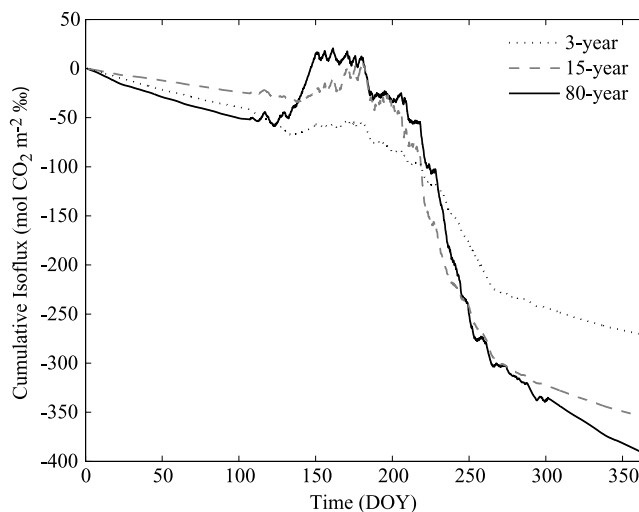

Figure 9. Cumulative net annual isoflux at the 3-year stand, 15-year stand, and 80-year stand. All stands are predicted to deplete the atmosphere in $\delta^{18}O$-CO_2 because ecosystem water pools in the far north are extremely depleted in $\delta^{18}O$. The atmospheric $\delta^{18}O$-CO_2 is not in steady state with surface water pools at this latitude owing to mixing with southern air masses with higher $\delta^{18}O$-CO_2.

Table 3. Sensitivity Analysis of the δ^{18}O-CO₂ Seasonal Cycle

Model Simulation	GPP Isoforcing, mol m^{-2} yr^{-1} ‰	R$_e$ Isoforcing, mol m^{-2} yr^{-1} ‰	Net Isoforcing, mol m^{-2} yr^{-1} ‰	δ^{18}O-CO₂ Amplitude, ‰	Percent Amplitude Change	Zero Crossing Point	Day Shift
Control, C_c/C_a = 0.76 time varying	227	−581	−354	1.2	0%	229	0
C_c/C_a = 0.76 constant	457	−581	−124	0.8	−33%	256	−17
C_c/C_a = 0.66 time varying	226	−581	−355	1.0	−17%	224	5
C_c/C_a = 0.86 time varying	213	−581	−368	1.9	58%	233	−4

adjustments to the GPP isoforcing were canceled out when integrated over the growing season.

5. Discussion

5.1. Disturbance-Induced Changes in CO₂ Seasonal Amplitude and Phase

[44] We compared seasonal carbon exchange from the 15-year and 80-year stands to test the *Zimov et al.* [1999] hypothesis that disturbance could contribute substantially to the observed increase in the seasonal amplitude of atmospheric CO₂. Previous work from a boreal forest chronosequence in Canada showed that light-saturated CO₂ uptake in midsummer is greatest in intermediate stand ages [*Litvak et al.*, 2003]. *Falge et al.* [2002] found that in temperate regions, broadleaf deciduous forest stands have a substantially shorter growing season that is characterized by high rates of net carbon uptake as compared with evergreen conifer forest stands. We measured an 85% increase in carbon uptake at the 15-year stand compared to the 80-year stand during the 31-day period from 18 June to 15 July (DOY 169–196). Together, these observations provide qualitative support for the *Zimov et al.* [1999] hypothesis, and the idea that plant functional type plays a key role in shaping the seasonal cycle of atmospheric CO₂ at high northern latitudes.

[45] In terms of explaining observed increases in the CO₂ amplitude in the Arctic from 1961–1994 [*Keeling et al.*, 1996], several factors suggest that disturbance-driven change in plant functional type within boreal ecosystems is probably not the dominant mechanism. From our one-box conceptual atmospheric model, replacing fluxes from the 80-year stand with fluxes from the 15-year stand caused an increase in the seasonal amplitude of CO₂ of 30%. This change represents a rough first guess at the expected effect of replacing all northern evergreen conifer forests with deciduous broadleaf forests. There is growing evidence that disturbance rates have increased in recent decades within the boreal forests of North America [*Kurz and Apps*, 1999; *Kasischke and Stocks*, 2000; *Gillett et al.*, 2004] and Eurasia [*Conard et al.*, 2002; *Sukhinin et al.*, 2004]; however, actual shifts in the distribution of stand ages and plant functional types have been far more modest than the total stand replacement represented by our model simulations. In addition, only 42% of the seasonal cycle at Point Barrow and other Arctic observation stations originates from biosphere-atmosphere exchange with boreal forests; tundra ecosystems contribute another 14%, deciduous forests contribute 12%, and grassland ecosystems farther to the south contribute another 16% [*Randerson et al.*, 1997].

[46] Another metric of seasonal cycle change is the phase, which is often measured by the DOY that the seasonal cycle

crosses from a positive value to a negative value in the spring (for a time series of CO₂ for which the secular trend from fossil fuel emissions has been removed). This "downward zero crossing time" of the atmospheric CO₂ seasonal cycle has advanced 7 days from 1975 to 1994 [*Keeling et al.*, 1996]. The leading candidate for explaining both the advanced CO₂ phase as well as increased amplitude is increasing spring and summer air temperature at high northern latitudes [*Keeling et al.*, 1996; *McDonald et al.*, 2004; *Angert et al.*, 2005]. A warmer climate simultaneously increases growing season length through earlier initiation of photosynthetic activity [*Black et al.*, 2000; *Tanja et al.*, 2003; *White and Nemani*, 2003] and net uptake rates during summer, and provides greater substrate for respiratory
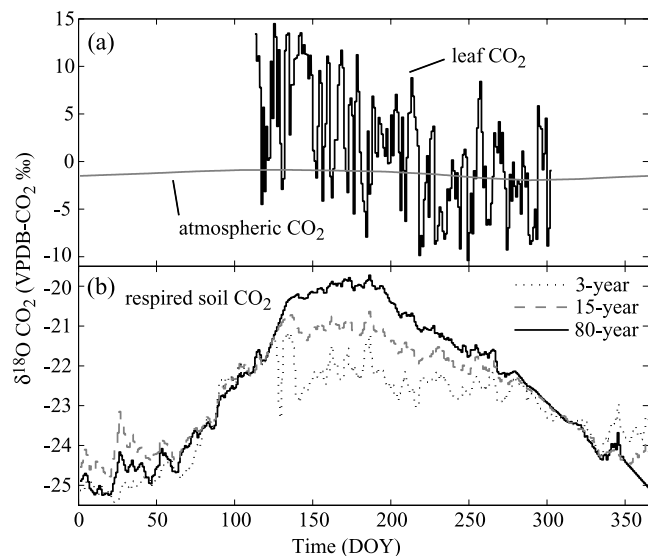

Figure 10. (a) Daily GPP-weighted leaf δ^{18}O-CO₂ and δ^{18}O of atmospheric CO₂ ($\delta_{a,i}^{CO_2}$) and (b) daily R$_e$-weighted respired soil δ^{18}O-CO₂ (diffusion fractionation of −7.2‰ has been included, $\delta_{soil}^{CO_2} - \varepsilon_{diff}$) for the 15-year stand. Maximum leaf CO₂ (and leaf water) δ^{18}O values in the beginning of the growing season (~DOY 150) were due to low humidity levels during this period (Figure 1c). This resulted in more positive Δ_A values on average earlier in the growing season and decreasing Δ_A toward the end of the season. Differences in the magnitude and seasonal distribution of GPP at each stand resulted in variations in the isoforcing among stands, even though the modeled δ^{18}O of leaf water was similar across stands. Soil temperature differences resulted in different equilibrium fractionation factors between CO₂ and water, and therefore δ^{18}O of soil respired CO₂ at each stand.

losses during fall, winter, and spring [*Goulden et al.*, 1998]. However, deciduous broadleaf trees must grow new leaves each spring, and hence there is a delay in the start of the carbon uptake period as compared with evergreen conifers that retain needles year round. This directly delays the phase of the CO_2 seasonal cycle, by 13 days at the 15-year stand compared to the 80-year. Using arguments similar to those discussed earlier for the CO_2 amplitude, we present this as an upper bound of expected atmospheric change if all boreal evergreen forests were replaced by deciduous forests. Assuming a modest increase in the rate of disturbance, we predict a shift toward deciduous forest species should have delayed the seasonal CO_2 phase by perhaps a day or two. This suggests that spring warming may have advanced the phase of the seasonal cycle of CO_2 even more than that predicted in previous studies that did not account for disturbance-induced change in forest stand age and plant functional type.

5.2. Factors Controlling the Seasonal Cycle of $\delta^{18}O$-CO_2

[47] The modeled amplitudes of the $\delta^{18}O$-CO_2 seasonal cycle imposed by surface fluxes at the 15-year stand and the 80-year stand were comparable (Figure 7b). Nonetheless, the phase and shape of the seasonal cycle was considerably different as a result of differences in isotopic exchange between the two stands. The $\delta^{18}O$-CO_2 phase was advanced by 9 days at the 15-year stand relative to the 80-year stand (Figure 7b). Stand-level differences in both the GPP and R_e isotopic fluxes contributed to differences in the phase and shape of the seasonal cycle (Figures 8e and 8f).

[48] Because precipitation is considerably depleted in ^{18}O at high northern latitudes, CO_2 in equilibrium with leaf water is close to atmospheric $\delta^{18}O$-CO_2 (Figure 10a). The GPP isoforcing was only slightly positive and was even negative at times (when the $\delta^{18}O$ of leaf CO_2 is less than $\delta_{a,i}^{CO_2}$), depleting the atmosphere in $\delta^{18}O$-CO_2. The flux-weighted annual mean Δ_A was +5.1‰ for the 15-year stand and +7.5‰ for the 80-year stand. For comparison, these Δ_A values were lower than other widely variable high-latitude estimates. *Farquhar et al.* [1993] predicted approximately +14‰ at 60°N, and *Flanagan et al.* [1997] estimated Δ_A was +21‰ for the Canadian boreal forest during midday in July which was also higher than our model predictions of midday Δ_A during July of approximately +17‰.

[49] In the Delta Junction study region, low spring relative humidity (Figure 1c) led to enriched leaf waters that gradually became more depleted as humidity increased throughout the summer (Figure 10a). Earlier initiation of GPP at the 80-year stand during the period of more enriched leaf water resulted in a more positive Δ_A at that stand. Delays in leaf out at the 15-year stand led to less atmospheric enrichment associated with GPP in the early part of the growing season (Figure 8c). Thus the increase in $\delta^{18}O$-CO_2 between April and June was considerably smaller for the 15-year stand as compared with the 80-year stand (Figures 7b and 8e). Changes in the phase also reflected differences in isotopic fluxes associated with R_e (Figure 8f). Specifically, the advance in phase of R_e at the 15-year stand (Figure 8b) led to an advance in the phase of the R_e isoforcing (Figure 8f).

[50] The phase of the seasonal cycle of $\delta^{18}O$-CO_2, most notably the minimum, is delayed from that of CO_2 by 1 to 2 months in the atmosphere at high northern latitudes [*Ciais and Meijer*, 1998; *Peylin et al.*, 1999]. Reproducing this phase lag in global models has been challenging and has been attributed in part to errors associated with atmospheric transport [*Cuntz et al.*, 2003b]. Our analysis suggests that ecosystem processes (independent of transport) may contribute to phase delays between $\delta^{18}O$-CO_2 and CO_2. Specifically, with our one-box atmospheric model, seasonal phases from the 80-year and 15-year stands showed a 1- or 2-month lag, respectively, between CO_2 and $\delta^{18}O$-CO_2 minima (Figure 7), matching the phase lag observed at Point Barrow. Preliminary analysis suggests that key controls on the phase at the ecosystem level include the isotopic composition of precipitation and seasonal patterns of plant water use.

5.3. Future Work

[51] We developed a simple model for $\delta^{18}O$-CO_2 isoforcing to extend the interpretation of our field measurements and to specifically investigate some of the effects of stand age on the seasonal cycle of $\delta^{18}O$-CO_2. In this analysis, we simplified or omitted a number of processes that should be considered in future work. First, there is an active area of research currently focusing on non-steady-state leaf water enrichment models and observations [*Cernusak et al.*, 2004; *Farquhar and Cernusak*, 2005] and the effects on canopy vapor $\delta^{18}O$ [*Lai et al.*, 2006] and surface isofluxes [*Seibt et al.*, 2006]. Differences in leaf morphology are likely to lead to different leaf water turnover times among broadleaves and conifer needles. More field experiments are required to accurately determine differences in the τ parameter (equation (2)). Recent work suggests nonzero nighttime stomatal conductance rates may have consequences for $\delta^{18}O$-CO_2 isofluxes and that the magnitude of the effect may be different for broadleaf and conifer species [*Barbour et al.*, 2005]. However, the degree to which concurrent increases in nighttime leaf and canopy boundary layer resistances offsets the impact of this mechanism for ecosystem $\delta^{18}O$-CO_2 isofluxes remains unexplored.

[52] A more complete representation of R_e isoforcing may be obtained, in future, by partitioning foliar and stem components of R_e [*Flanagan et al.*, 1997; *Bowling et al.*, 2003a, 2003b; *Riley et al.*, 2003] and by including the effects of moss water on soil R_e isoforcing [e.g., *Flanagan et al.*, 1997]. R_e isoforcing estimates could also be improved by including a more detailed representation of equilibration of CO_2 with surface soil water pools [*Riley et al.*, 2002] and fluxes associated with abiotic atmosphere-soil CO_2 exchange [*Tans*, 1998; *Miller et al.*, 1999; *Stern et al.*, 2001]. A key factor that contributes to uncertainty in the GPP isoforcing term is our limited understanding of seasonal patterns of plant water use, including the use of snowmelt water by different plant species throughout the growing season [*Sugimoto et al.*, 2002; *Welp et al.*, 2005].

6. Conclusions

[53] We measured NEE and the isotopic composition of atmosphere and ecosystem water pools at three stands in a boreal forest fire chronosequence. Our measurements and

model analysis provide evidence that species composition exerts a strong control on the shape of both the CO_2 and $\delta^{18}O$-CO_2 seasonal cycles at high northern latitudes. An expansion of the areas covered by deciduous forests in the boreal region, as a result of increased forest fire frequency, would increase the amplitude and delay the phase of the seasonal cycle of CO_2. Increases in high-latitude disturbance and spring warming have been proposed as potential explanations of observed increases in the amplitude of the seasonal cycle of atmospheric CO_2 [*Keeling et al.*, 1996; *Zimov et al.*, 1999; *McDonald et al.*, 2004; *Angert et al.*, 2005]. Our work implies that it must be a combination of these processes. Changes in the boreal disturbance regime over the last few decades, though not well characterized, seem too small to drive large changes in the seasonal amplitude, on the basis of our NEE measurements.

[54] Our analysis also provides evidence that the seasonal cycle of $\delta^{18}O$-CO_2 is sensitive to the seasonal timing of GPP and R_e surface fluxes, both of which are controlled by plant functional type (and thus stand age) within the boreal forest. In contrast to CO_2, an expansion of the areas covered by deciduous forests would advance the phase of the $\delta^{18}O$-CO_2 seasonal cycle. An increase in deciduous forest area would also weaken GPP isoforcing during the early part of the growing season and cause $\delta^{18}O$-CO_2 to increase more gradually between April and June. Important next steps include improving our understanding winter and summer precipitation use by different plant functional types and investigating the impact of changing plant functional types and climate on the $\delta^{18}O$-CO_2 seasonal cycle using a coupled model that includes atmospheric transport and mixing.

References

Angert, A., S. Biraud, A. Bonfils, C. C. Henning, W. Buermann, J. Pinzon, C. J. Tucker, and I. Fung (2005), Drier summers cancel out the CO_2 uptake enhancement induced by warmer springs, *Proc. Natl. Acad. Sci. U. S. A.*, *102*(31), 10,823–10,827.

Arctic Climate Impact Assessment (2004), *Impacts of a Warming Arctic: Arctic Climate Impact Assessment*, Cambridge Univ. Press, New York.

Ball, J. T. (1988), An analysis of stomatal conductance, Ph.D. thesis, Stanford Univ., Stanford, Calif.

Barbour, M. M., L. A. Cernusak, D. Whitehead, K. L. Griffin, M. H. Turnbull, D. T. Tissue, and G. D. Farquhar (2005), Nocturnal stomatal conductance and implications for modelling delta O-18 of leaf-respired CO_2 in temperate tree species, *Funct. Plant Biol.*, *32*(12), 1107–1121.

Black, T. A., W. J. Chen, A. G. Barr, M. A. Arain, Z. Chen, Z. Nesic, E. H. Hogg, H. H. Neumann, and P. C. Yang (2000), Increased carbon sequestration by a boreal deciduous forest in years with a warm spring, *Geophys. Res. Lett.*, *27*(9), 1271–1274.

Bogaert, J., L. Zhou, C. J. Tucker, R. B. Myneni, and R. Ceulemans (2002), Evidence for a persistent and extensive greening trend in Eurasia inferred from satellite vegetation index data, *J. Geophys. Res.*, *107*(D11), 4119, doi:10.1029/2001JD001075.

Bolin, B., and C. D. Keeling (1963), Large-scale atmospheric mixing as deduced from seasonal and meridional variations of carbon dioxide, *J. Geophys. Res.*, *68*(13), 3899–3920.

Bond-Lamberty, B., C. K. Wang, and S. T. Gower (2004), Net primary production and net ecosystem production of a boreal black spruce wildfire chronosequence, *Global Change Biol.*, *10*, 473–487.

Bowling, D. R., N. G. McDowell, J. M. Welker, B. J. Bond, B. E. Law, and J. R. Ehleringer (2003a), Oxygen isotope content of CO_2 in nocturnal ecosystem respiration: 1. Observations in forests along a precipitation transect in Oregon, USA, *Global Biogeochem. Cycles*, *17*(4), 1120, doi:10.1029/2003GB002081.

Bowling, D. R., N. G. McDowell, J. M. Welker, B. J. Bond, B. E. Law, and J. R. Ehleringer (2003b), Oxygen isotope content of CO_2 in nocturnal ecosystem respiration: 2. Short-term dynamics of foliar and soil component fluxes in an old-growth ponderosa pine forest, *Global Biogeochem. Cycles*, *17*(4), 1124, doi:10.1029/2003GB002082.

Cappa, C. D., M. B. Hendricks, D. J. DePaolo, and R. C. Cohen (2003), Isotopic fractionation of water during evaporation, *J. Geophys. Res.*, *108*(D16), 4525, doi:10.1029/2003JD003597.

Cernusak, L. A., G. D. Farquhar, S. C. Wong, and H. Stuart-Williams (2004), Measurement and interpretation of the oxygen isotope composition of carbon dioxide respired by leaves in the dark, *Plant Physiol.*, *136*(2), 3350–3363.

Cess, R. D., et al. (1991), Interpretation of snow-climate feedback as produced by 17 general-circulation models, *Science*, *253*(5022), 888–892.

Chapin, F. S., S. A. Zimov, G. R. Shaver, and S. E. Hobbie (1996), CO_2 fluctuation at high latitudes, *Nature*, *383*(6601), 585–586.

Ciais, P., and H. A. J. Meijer (1998), The $^{18}O/^{16}O$ isotope ratio of atmospheric CO_2 and its role in global carbon cycle research, in *Stable Isotopes*, pp. 409–431, BIOS Sci., Oxford, U.K.

Ciais, P., et al. (1997), A three-dimensional synthesis study of delta O-18 in atmospheric CO_2: 1. Surface fluxes, *J. Geophys. Res.*, *102*(D5), 5857–5872.

Conard, S. G., A. I. Sukhinin, B. J. Stocks, D. R. Cahoon, E. P. Davidenko, and G. A. Ivanova (2002), Determining effects of area burned and fire severity on carbon cycling and emissions in Siberia, *Clim. Change*, *55*(1–2), 197–211.

Conway, T. J., P. P. Tans, L. S. Waterman, and K. W. Thoning (1994), Evidence for interannual variability of the carbon cycle from the National Oceanic and Atmospheric Administration/Climate Monitoring and Diagnostics Laboratory Global Air Sampling Network, *J. Geophys. Res.*, *99*(D11), 22,831–22,855.

Craig, H., and L. I. Gordon (1965), Deuterium and oxygen-18 variations in the ocean and the marine atmosphere, paper presented at Proceedings of a Conference on Stable Isotopes in Oceanographic Studies and Paleotemperatures, Lab. Geol. Nucl., Spoleto, Italy.

Cuntz, M., P. Ciais, G. Hoffmann, C. E. Allison, and W. Knorr (2003a), A comprehensive global three-dimensional model of delta O-18 in atmospheric CO_2: 1. Validation of surface processes, *J. Geophys. Res.*, *108*(D17), 4527, doi:10.1029/2002JD003153.

Cuntz, M., P. Ciais, G. Hoffmann, C. E. Allison, R. J. Francey, W. Knorr, P. P. Tans, J. W. C. White, and I. Levin (2003b), A comprehensive global three-dimensional model of delta O-18 in atmospheric CO_2: 2. Mapping the atmospheric signal, *J. Geophys. Res.*, *108*(D17), 4528, doi:10.1029/2002JD003154.

Dang, Q. L., H. A. Margolis, M. R. Coyea, M. Sy, and G. J. Collatz (1997), Regulation of branch-level gas exchange of boreal trees: Roles of shoot water potential and vapor pressure difference, *Tree Physiol.*, *17*(8–9), 521–535.

Dongmann, G., H. W. Nurnberg, H. Forstel, and K. Wagener (1974), Enrichment of $H_2^{18}O$ in leaves of transpiring plants, *Radiat. Environ. Biophys.*, *11*(1), 41–52.

Ehleringer, J. R., J. Roden, and T. E. Dawson (2000), Assessing ecosystem-level water relations through stable isotope ratio analysis, in *Methods in Ecosystem Science*, pp. 181–198, Springer, New York.

Ewers, B. E., S. T. Gower, B. Bond-Lamberty, and C. K. Wang (2005), Effects of stand age and tree species on canopy transpiration and average stomatal conductance of boreal forests, *Plant Cell Environ.*, *28*(5), 660–678.

Falge, E., et al. (2002), Phase and amplitude of ecosystem carbon release and uptake potentials as derived from FLUXNET measurements, *Agric. For. Meteorol.*, *113*(1–4), 75–95.

Farquhar, G. D., and L. A. Cernusak (2005), On the isotopic composition of leaf water in the non-steady state, *Funct. Plant Biol.*, *32*(4), 293–303.

Farquhar, G. D., J. R. Ehleringer, and K. T. Hubick (1989), Carbon isotope discrimination and photosynthesis, *Annu. Rev. Plant Physiol. Plant Mol. Biol.*, *40*, 503–537.

Farquhar, G. D., J. Lloyd, J. A. Taylor, L. B. Flanagan, J. P. Syvertsen, K. T. Hubick, S. C. Wong, and J. R. Ehleringer (1993), Vegetation effects on

the isotope composition of oxygen in atmospheric CO_2, *Nature*, *363*(6428), 439–443.

Fessenden, J. E., C. S. Cook, M. J. Lott, and J. R. Ehleringer (2002), Rapid ^{18}O analysis of small water and CO_2 samples using a continuous-flow isotope ratio mass spectrometer, *Rapid Commun. Mass Spectrom.*, *16*, 1257–1260.

Flanagan, L. B. (2005), Ecosystem CO_2 exchange and variation in the $\delta^{18}O$ of atmospheric CO_2, in *Stable Isotopes and Biosphere-Atmosphere Interactions: Processes and Biological Controls*, pp. 171–181, Elsevier, New York.

Flanagan, L. B., J. P. Comstock, and J. R. Ehleringer (1991), Comparison of modeled and observed environmental-influences on the stable oxygen and hydrogen isotope composition of leaf water in *Phaseolus vulgaris* L., *Plant Physiol.*, *96*(2), 588–596.

Flanagan, L. B., J. R. Brooks, G. T. Varney, and J. R. Ehleringer (1997), Discrimination against (COO)-O-18-O-16 during photosynthesis and the oxygen isotope ratio of respired CO_2 in boreal forest ecosystems, *Global Biogeochem. Cycles*, *11*(1), 83–98.

Flannigan, M. D., K. A. Logan, B. D. Amiro, W. R. Skinner, and B. J. Stocks (2005), Future area burned in Canada, *Clim. Change*, *72*(1–2), 1–16.

Francey, R. J., and P. P. Tans (1987), Latitudinal variation in O-18 of atmospheric CO_2, *Nature*, *327*(6122), 495–497.

Friedli, H., U. Siegenthaler, D. Rauber, and H. Oeschger (1987), Measurements of concentration, $^{13}C/^{12}C$ and $^{18}O/^{16}O$ ratios of tropospheric carbon dioxide over Switzerland, *Tellus, Ser. B*, *39*, 80–88.

Frolking, S., et al. (1996), Modelling temporal variability in the carbon balance of a spruce/moss boreal forest, *Global Change Biol.*, *2*, 343–366.

Gillett, N. P., A. J. Weaver, F. W. Zwiers, and M. D. Flannigan (2004), Detecting the effect of climate change on Canadian forest fires, *Geophys. Res. Lett.*, *31*, L18211, doi:10.1029/2004GL020876.

Gillon, J., and D. Yakir (2001), Influence of carbonic anhydrase activity in terrestrial vegetation on the O-18 content of atmospheric CO_2, *Science*, *291*(5513), 2584–2587.

Goulden, M. L., B. C. Daube, S. M. Fan, D. J. Sutton, A. Bazzaz, J. W. Munger, and S. C. Wofsy (1997), Physiological responses of a black spruce forest to weather, *J. Geophys. Res.*, *102*(D24), 28,987–28,996.

Goulden, M. L., et al. (1998), Sensitivity of boreal forest carbon balance to soil thaw, *Science*, *279*(5348), 214–217.

Helliker, B. R., J. S. Roden, C. Cook, and J. R. Ehleringer (2002), A rapid and precise method for sampling and determining the oxygen isotope ratio of atmospheric water vapor, *Rapid Commun. Mass Spectrom.*, *16*, 929–932.

Hesterberg, R., and U. Siegenthaler (1991), Production and stable isotopic composition of CO_2 in a soil near Bern, Switzerland, *Tellus, Ser. B*, *43*, 197–205.

Hicke, J. A., G. P. Asner, J. T. Randerson, C. Tucker, S. Los, R. Birdsey, J. C. Jenkins, and C. Field (2002), Trends in North American net primary productivity derived from satellite observations, 1982–1998, *Global Biogeochem. Cycles*, *16*(2), 1018, doi:10.1029/2001GB001550.

Intergovernmental Panel on Climate Change (2001), *Climate Change 2001*, Cambridge Univ. Press, New York.

Jarvis, P. G., and K. G. McNaughton (1986), Stomatal control of transpiration: Scaling up from leaf to region, in *Advances in Ecological Research*, pp. 1–49, Elsevier, New York.

Kasischke, E. S., and B. J. Stocks (2000), *Fire, Climate Change, and Carbon Cycling in the Boreal Forest*, 461 pp., Springer, New York.

Keeling, C. D., J. F. S. Chin, and T. P. Whorf (1996), Increased activity of northern vegetation inferred from atmospheric CO_2 measurements, *Nature*, *382*(6587), 146–149.

Kimball, J. S., K. C. McDonald, A. R. Keyser, S. Frolking, and S. W. Running (2001), Application of the NASA scatterometer (NSCAT) for determining the daily frozen and nonfrozen landscape of Alaska, *Remote Sens. Environ.*, *75*(1), 113–126.

King, S., J. Harden, K. L. Manies, J. Munster, and D. L. White (2002), Fate of carbon in Alaskan landscapes project—Database for soils from eddy covariance tower sites, Delta Junction, AK, *Open File Rep. 02-62*, U.S Geol. Surv., Menlo Park, Calif.

Kurz, W. A., and M. J. Apps (1999), A 70-year retrospective analysis of carbon fluxes in the Canadian forest sector, *Ecol. Appl.*, *9*, 526–547.

Lai, C. T., J. R. Ehleringer, B. J. Bond, and K. T. Paw U (2006), Contributions of evaporation, isotopic non-steady state transpiration and atmospheric mixing on the delta O-18 of water vapour in Pacific Northwest coniferous forests, *Plant Cell Environ.*, *29*(1), 77–94.

Litvak, M., S. Miller, S. C. Wofsy, and M. Goulden (2003), Effect of stand age on whole ecosystem CO_2 exchange in the Canadian boreal forest, *J. Geophys. Res.*, *108*(D3), 8225, doi:10.1029/2001JD000854.

Liu, H. P., G. Peters, and T. Foken (2001), New equations for sonic temperature variance and buoyancy heat flux with an omnidirectional sonic anemometer, *Boundary Layer Meteorol.*, *100*(3), 459–468.

Liu, H. P., J. T. Randerson, J. Lindfors, and F. S. Chapin (2005), Changes in the surface energy budget after fire in boreal ecosystems of interior Alaska: An annual perspective, *J. Geophys. Res.*, *110*, D13101, doi:10.1029/2004JD005158.

Lloyd, J., and G. D. Farquhar (1994), C-13 discrimination during CO_2 assimilation by the terrestrial biosphere, *Oecologia*, *99*(3–4), 201–215.

Lloyd, J., and J. A. Taylor (1994), On the temperature-dependence of soil respiration, *Funct. Ecol.*, *8*(3), 315–323.

Manies, K. L., J. W. Harden, S. R. Silva, P. H. Briggs, and B. M. Schmid (2004), Soil data from *Picea mariana* stands near Delta Junction, Alaska of different ages and soil drainage type, *U.S. Geol. Surv. Open File Rep.*, *2004-1271*, 19 pp.

McDonald, K. C., J. S. Kimball, E. Njoku, R. Zimmermann, and Z. Maosheng (2004), Variability in springtime thaw in the terrestrial high latitudes: Monitoring a major control on the biospheric assimilation of atmospheric CO_2 with spaceborne microwave remote sensing, *Earth Interact.*, *8*(20), 1–23.

Menzel, A., and P. Fabian (1999), Growing season extended in Europe, *Nature*, *397*(6721), 659.

Miller, J. B., D. Yakir, J. W. C. White, and P. P. Tans (1999), Measurement of O-18/O-16 in the soil-atmosphere CO_2 flux, *Global Biogeochem. Cycles*, *13*(3), 761–774.

Mills, G. A., and H. C. Urey (1940), The kinetics of isotopic exchange between carbon dioxide, bicarbonate ion, carbonate ion and water, *J. Am. Chem. Soc.*, *62*, 1019–1026.

Myneni, R. B., C. D. Keeling, C. J. Tucker, G. Asrar, and R. R. Nemani (1997), Increased plant growth in the northern high latitudes from 1981 to 1991, *Nature*, *386*(6626), 698–702.

Myneni, R. B., et al. (2002), Global products of vegetation leaf area and fraction absorbed PAR from year one of MODIS data, *Remote Sens. Environ.*, *83*(1–2), 214–231.

Nemani, R. R., C. D. Keeling, H. Hashimoto, W. M. Jolly, S. C. Piper, C. J. Tucker, R. B. Myneni, and S. W. Running (2003), Climate-driven increases in global terrestrial net primary production from 1982 to 1999, *Science*, *300*(5625), 1560–1563.

Ogee, J., P. Peylin, M. Cuntz, T. Bariac, Y. Brunet, P. Berbigier, P. Richard, and P. Ciais (2004), Partitioning net ecosystem carbon exchange into net assimilation and respiration with canopy-scale isotopic measurements: An error propagation analysis with (CO_2)-C-13 and (COO)-O-18 data, *Global Biogeochem. Cycles*, *18*, GB2019, doi:10.1029/2003GB002166.

O'Neill, K. P., E. S. Kasischke, and D. D. Richter (2003), Seasonal and decadal patterns of soil carbon uptake and emission along an age sequence of burned black spruce stands in interior Alaska, *J. Geophys. Res.*, *108*(D1), 8155, doi:10.1029/2001JD000443.

Peylin, P., P. Ciais, A. S. Denning, P. P. Tans, J. A. Berry, and J. W. C. White (1999), A 3-dimensional study of delta O-18 in atmospheric CO_2: Contribution of different land ecosystems, *Tellus, Ser. B*, *51*, 642–667.

Randerson, J. T., M. V. Thompson, T. J. Conway, I. Y. Fung, and C. B. Field (1997), The contribution of terrestrial sources and sinks to trends in the seasonal cycle of atmospheric carbon dioxide, *Global Biogeochem. Cycles*, *11*(4), 535–560.

Randerson, J. T., C. B. Field, I. Y. Fung, and P. P. Tans (1999), Increases in early season ecosystem uptake explain recent changes in the seasonal cycle of atmospheric CO_2 at high northern latitudes, *Geophys. Res. Lett.*, *26*(17), 2765–2768.

Riley, W. J., C. J. Still, M. S. Torn, and J. A. Berry (2002), A mechanistic model of (H_2O)-O-18 and (COO)-O-18 fluxes between ecosystems and the atmosphere: Model description and sensitivity analyses, *Global Biogeochem. Cycles*, *16*(4), 1095, doi:10.1029/2002GB001878.

Riley, W. J., C. J. Still, B. R. Helliker, M. Ribas-Carbo, and J. A. Berry (2003), O-18 composition of CO_2 and H_2O ecosystem pools and fluxes in a tallgrass prairie: Simulations and comparisons to measurements, *Global Change Biol.*, *9*, 1567–1581.

Seibt, U., L. Wingate, J. A. Berry, and J. Lloyd (2006), Non-steady state effects in diurnal ^{18}O discrimination by *Picea sitchensis* branches in the field, *Plant Cell Environ.*, *29*(5), doi:10.1111/j.1365-3040.2005.01474.x.

Slayback, D. A., J. E. Pinzon, S. O. Los, and C. J. Tucker (2003), Northern Hemisphere photosynthetic trends 1982–99, *Global Change Biol.*, *9*, 1–15.

Smith, N. V., S. S. Saatchi, and J. T. Randerson (2004), Trends in high northern latitude soil freeze and thaw cycles from 1988 to 2002, *J. Geophys. Res.*, *109*, D12101, doi:10.1029/2003JD004472.

Stern, L. A., R. Amundson, and W. T. Baisden (2001), Influence of soils on oxygen isotope ratio of atmospheric CO_2, *Global Biogeochem. Cycles*, *15*(3), 753–759.

Stocks, B. J., et al. (1998), Climate change and forest fire potential in Russian and Canadian boreal forests, *Clim. Change*, *38*(1), 1–13.

Sugimoto, A., N. Yanagisawa, D. Naito, N. Fujita, and T. C. Maximov (2002), Importance of permafrost as a source of water for plants in east Siberian taiga, *Ecol. Res.*, *17*(4), 493–503.

Sukhinin, A. I., et al. (2004), AVHRR-based mapping of fires in Russia: New products for fire management and carbon cycle studies, *Remote Sens. Environ.*, *93*(4), 546–564.

Tanja, S., et al. (2003), Air temperature triggers the recovery of evergreen boreal forest photosynthesis in spring, *Global Change Biol.*, *9*, 1410–1426.

Tans, P. P. (1998), Oxygen isotopic equilibrium between carbon dioxide and water in soils, *Tellus, Ser. B*, *50*, 163–178.

Trolier, M., J. W. C. White, P. P. Tans, K. A. Masarie, and P. A. Gemery (1996), Monitoring the isotopic composition of atmospheric CO_2: Measurements from the NOAA Global Air Sampling Network, *J. Geophys. Res.*, *101*(D20), 25,897–25,916.

Tucker, C. J., D. A. Slayback, J. E. Pinzon, S. O. Los, R. B. Myneni, and M. G. Taylor (2001), Higher northern latitude normalized difference vegetation index and growing season trends from 1982 to 1999, *Int. J. Biometeorol.*, *45*(4), 184–190.

Walther, G. R., E. Post, P. Convey, A. Menzel, C. Parmesan, T. J. C. Beebee, J. M. Fromentin, O. Hoegh-Guldberg, and F. Bairlein (2002), Ecological responses to recent climate change, *Nature*, *416*(6879), 389–395.

Wang, C. K., B. Bond-Lamberty, and S. T. Gower (2002), Soil surface CO_2 flux in a boreal black spruce fire chronosequence, *J. Geophys. Res.*, *107*, 8224, doi:10.1029/2001JD000861. [printed *108*(D3), 2003]

Webb, E. K., G. I. Pearman, and R. Leuning (1980), Correction of flux measurements for density effects due to heat and water-vapor transfer, *Q. J. R. Meteorol. Soc.*, *106*(447), 85–100.

Welp, L. R., J. T. Randerson, J. C. Finlay, S. P. Davydov, G. M. Zimova, A. I. Davydova, and S. A. Zimov (2005), A high-resolution time series of oxygen isotopes from the Kolyma River: Implications for the seasonal dynamics of discharge and basin-scale water use, *Geophys. Res. Lett.*, *32*, L14401, doi:10.1029/2005GL022857.

White, M. A., and A. R. Nemani (2003), Canopy duration has little influence on annual carbon storage in the deciduous broad leaf forest, *Global Change Biol.*, *9*, 967–972.

Yakir, D., and L. Sternberg (2000), The use of stable isotopes to study ecosystem gas exchange, *Oecologia*, *123*, 297–311.

Yakir, D., and X. F. Wang (1996), Fluxes of CO_2 and water between terrestrial vegetation and the atmosphere estimated from isotope measurements, *Nature*, *380*(6574), 515–517.

Zha, T., S. Kellomaki, K. Y. Wang, and I. Rouvinen (2004), Carbon sequestration and ecosystem respiration for 4 years in a Scots pine forest, *Global Change Biol.*, *10*, 1492–1503.

Zhou, L. M., C. J. Tucker, R. K. Kaufmann, D. Slayback, N. V. Shabanov, and R. B. Myneni (2001), Variations in northern vegetation activity inferred from satellite data of vegetation index during 1981 to 1999, *J. Geophys. Res.*, *106*(D17), 20,069–20,083.

Zimov, S. A., S. P. Davidov, G. M. Zimova, A. I. Davidova, F. S. Chapin, M. C. Chapin, and J. F. Reynolds (1999), Contribution of disturbance to increasing seasonal amplitude of atmospheric CO_2, *Science*, *284*(5422), 1973–1976.

———————————

H. P. Liu, Department of Physics, Atmospheric Sciences, and General Science, Jackson State University, P.O. Box 17660, Jackson, MS 39217, USA. (heping.liu@jsums.edu)

J. T. Randerson, Earth System Science, University of California, Irvine, 3212 Croul Hall, Irvine, CA 92697, USA. (jranders@uci.edu)

L. R. Welp, Environmental Science and Engineering, California Institute of Technology, Mail Code 100-23, Pasadena, CA 91125, USA. (welp@caltech.edu)